NULISA: a novel proteomic liquid biopsy platform with attomolar sensitivity and high multiplexing

Wei Feng[1], Joanne Beer[1], Qinyu Hao[1], Ishara S Ariyapala[1], Aparna Sahajan[1], Andrei Komarov[1], Katie Cha[1], Mason Moua[1], Xiaolei Qiu[1], Xiaomei Xu[1], Shweta Iyengar[1], Thu Yoshimura[1], Rajini Nagaraj[1], Li Wang[1], Ming Yu[1], Kate Engel[1], Lucas Zhen[1], Wen Xue[1], Chen-jung Lee[1], Chan Ho Park[1], Cheng Peng[1], Kaiyuan Zhang[1], Adrian Grzybowski[1], Johnnie Hahm[1], Susanne V. Schmidt[2], Alexandru Odainic[2,3], Jasper Spitzer[2], Bonn COVIMMUNE Consortium, Kasun Buddika[1], Dwight Kuo[1], Lei Fang[1], Bingqing Zhang[1], Steve Chen[1], Eicke Latz[2], Yiyuan Yin[1], Yuling Luo[1]*, Xiao-Jun Ma[1]*

[1]Alamar Biosciences, Inc., Fremont, CA, USA
[2]Institute of Innate Immunity, Medical Faculty, University of Bonn, Bonn, Germany
[3]Department of Microbiology and Immunology, The Peter Doherty Institute for Infection and Immunity, University of Melbourne, Melbourne, Australia

***Correspondence:** xma@alamarbio.com; yluo@alamarbio.com

Keywords

Immunoassay; proteomics; antibodies; proximity ligation; multiplex; PCR; NGS; NULISA; PLA; liquid biopsy

Abstract

The blood proteome holds great promise for precision medicine but poses daunting challenges due to the low abundance of the majority of plasma proteins and the vast dynamic range across the proteome. We report the development and validation of a novel proteomic analysis technology – NUcleic acid Linked Immuno-Sandwich Assay (NULISA™) – that incorporates a dual capture and release mechanism to suppress the assay background to the minimum, thus drastically improving the signal-to-noise ratio. NULISA improves the sensitivity of the proximity ligation assay by over 10,000-fold to the attomolar level, which is enabled by antibody-conjugated DNA sequences that mediate the purification of immunocomplexes and contain target- and sample-specific barcodes for next-generation sequencing-based, highly multiplexed analysis. To demonstrate its performance and utility, we developed a 200-plex NULISA targeting 124 cytokines and chemokines and 80 other immune response-related proteins that demonstrated superior sensitivity for detecting low-abundance proteins and high concordance with other immunoassays. The ultra-high sensitivity enabled the detection of previously difficult-to-detect but biologically important, low-abundance biomarkers in patients with autoimmune diseases and COVID-19. Fully automated NULISA uniquely addresses longstanding challenges in the proteomic analysis of liquid biopsy samples and makes broad and in-depth proteomic analysis accessible to the general research community and future diagnostic applications.

Introduction

Blood has long been investigated as a universal liquid biopsy material in a wide range of clinical settings, including cancer and many serious chronic diseases[1,2]. The advent of next-generation DNA sequencing (NGS) technologies has ushered in a new era of DNA liquid biopsy, especially in the context of cancer, for which genetic and epigenetic alterations are routinely assessed using circulating cell-free tumor DNA (ctDNA) for a range of clinical applications[3,4]. However, the blood proteome is likely to hold even greater promise for providing a real-time snapshot of the functioning of the entire body. It is the most complex and comprehensive proteome because it contains not only actively secreted proteins but also the proteomes of other tissues due to tissue leakage as well as pathogens[5,6]. Proteins, as workhorses of all living systems, more closely reflect dynamic physiological and pathological processes[7] and are thus more broadly applicable as blood-based biomarkers for essentially every disease state. However, investigating the blood proteome has proven challenging due to the low concentrations (<1 pg/ml) of most proteins and the vast 12-log dynamic range of protein concentration[8]. To date, only ~150 of the estimated >10,000 plasma proteins are in diagnostic use[9]. To realize and leverage this vast source of biomarkers, major technological advances in both sensitivity and multiplexing are needed.

Currently, mass spectrometry (MS)[10] and immunoassays are the two pillars of proteomic analysis. MS-based methods are capable of de novo detection and quantification of hundreds to thousands of proteins, but they are biased toward high-abundance proteins (>1 ng/ml)[11] and have a narrow dynamic range (4-6 logs); thus, they cannot detect most clinically relevant biomarkers in routine settings. Immunoassays using a sandwich pair of antibodies to recognize a single target can achieve higher sensitivity, in the range of 1-10 pg/ml[11]; Some methods, including immuno-PCR[12], proximity ligation assay (PLA)[13,14], proximity extension assay (PEA)[15], single molecule array (SIMOA)[16], and single molecule counting (SMC)[17], are in fact capable of single-molecule detection. However, with complex real-world samples, the sensitivity of even the most advanced single-molecule

counting-based immunoassays remains inadequate to reach the low abundance portion of the plasma proteome.

Multiplexed immunoassays that measure multiple proteins in a single experiment can save both time and precious samples and improve precision. Increasing multiplexing levels to 100s and 1000s proteins can provide a more comprehensive view of the proteome than possible from a single protein or a few proteins, which can lead to new biological insights. However, they pose another considerable challenge. The Luminex bead-based immunoassay[18] quickly loses sensitivity and specificity when the level of multiplexing increases beyond 50 targets because of the exponential increase in potential cross-interactions between noncognate pairs of antibodies. Single affinity reagent-based methods, such as the SomaScan assay, can be easily scaled to enable high multiplexing but can be prone to false positive signals because of the reliance on a single aptamer binding event[19]. Recently, PEA in combination with NGS was shown to achieve highly specific and multiplexed detection of up to 384 proteins in a single reaction[20] through the incorporation of both target- and sample-specific barcodes into the reporter DNA and subsequent sequencing. However, PEA is not currently the most sensitive assay, and the assay protocol consists of numerous manual steps and requires multiple liquid-handling instruments, making it unsuitable for routine use, especially in clinical settings. Thus, high multiplexing without compromising sensitivity and specificity in a broadly accessible system remains an important unmet need.

Previously, we achieved robust single RNA molecule *in situ* detection with RNAscope[21], a technology that greatly improves detection sensitivity by suppressing background signals. We hypothesized that the same background suppression principle could be applied to immunoassays to improve protein detection sensitivity. Here, we report the development of NUcleic acid-Linked Immuno-Sandwich Assay (NULISA), which incorporates multiple mechanisms of background suppression. We assessed the analytical performance of this assay in detecting a panel of 204 proteins, including 124 cytokines, chemokines, and other key proteins involved in inflammation and immune response. We also demonstrated the ability of NULISA to detect previously difficult-to-

detect but biologically important, low-abundance biomarkers in patients with autoimmune diseases and COVID-19. NULISA's ultra-high sensitivity and high multiplexing in a fully automated platform should democratize both in-depth and broad analysis of the blood proteome to provide new biological insights into diseases and to discover a new generation of biomarkers for the earliest detection of serious diseases.

Results

NULISA background suppression enables attomolar level sensitivity

A critical design goal of NULISA is background suppression. We adopted the principle of PLA[13] but designed additional mechanisms in the DNA-antibody conjugate to suppress various background sources, resulting in the development of the NULISA protocol (**Fig. 1a**). In brief, the capture antibody is conjugated with partially double-stranded DNA containing a poly-A tail and a target-specific barcode, whereas the detection antibody is conjugated with another partially double-stranded DNA containing a biotin group and a matching target-specific barcode (**Fig. 1a-1**). When both antibodies are incubated with a sample containing the target molecule, an immunocomplex is formed. The formed immunocomplexes are captured by added paramagnetic oligo-dT beads and subsequent dT-polyA hybridization (**Fig. 1a-2**), and the sample matrix and unbound detection antibodies are removed by washing (**Fig. 1a-3**). As dT-polyA binding is sensitive to salt concentration, the formed immunocomplexes are then released into a low-salt buffer (**Fig. 1a-4**). After removing the dT beads, a second set of paramagnetic beads coated with streptavidin is introduced to capture the immunocomplexes in the solid phase a second time (**Fig. 1a-5**), allowing subsequent washes to remove free unbound capture antibodies, resulting in essentially pure immunocomplexes on the beads. Then, a ligation mix containing T4 DNA ligase and a specific DNA ligator sequence is added to the streptavidin beads, allowing the ligation of the proximal ends of DNA attached to the paired antibodies and thus generating a new DNA reporter molecule containing unique target-specific barcodes (**Fig. 1a-6**). The levels of the DNA reporter can then be quantified by quantitative PCR (qPCR) (**Fig. 1a-7a**) or NGS (**Fig. 1a-7b**). As this is a paramagnetic bead-based assay, the entire workflow can be readily automated from sample preparation to qPCR data acquisition or to the preparation of an NGS-ready library.

For NGS-based multiplexing, in addition to target-specific barcodes, sample-specific barcodes are introduced into reporter DNA using double-stranded ligators containing sample barcodes in the middle (**Fig. 1a-7b**), which enables pooling of a full 96-well plate of samples into one sequencing reaction. After ligation, the ligation products are pooled,

amplified, and purified to generate a sequencing library that is compatible with multiple Illumina sequencing instruments. Raw sequencing reads are processed to generate target- and sample-specific read counts. Raw read counts are normalized using spiked-in mCherry protein to control for potential well-to-well variation and an inter-plate control sample for plate-to-plate variation.

To demonstrate that background suppression in NULISA can result in improved sensitivity, we compared the IL4 detection performance of NULISA with a homogeneous PLA using the same set of antibody conjugates and assay buffer and a serial dilution of IL4 from 500 pM to 1 aM. Compared with traditional PLA, NULISA reduced the background by more than 10,000-fold, thereby achieving an attomolar-level limit of detection (LOD) and a 7-log dynamic range, corresponding to a greater than 4-log increase (**Fig. 1b**).

To further demonstrate that NULISA with background suppression can lead to better detection sensitivity than single-molecule detection technologies, we compared the performance of NULISA with that of SIMOA using the same pair of antibodies to detect human immunodeficiency virus (HIV) p24 protein spiked into healthy donor plasma. NULISA demonstrated a 10 aM LOD, which is nearly 10-fold lower than that of SIMOA (**Fig. 1c**); notably, SIMOA used 6x more sample input than NULISA (124 µL vs. 20 µL). In addition, NULISA detection of HIV p24 was demonstrated over a 7-log dynamic range, which was 3 logs wider than the range for SIMOA.

To demonstrate the specificity of NULISA, we determined the LOD for human EGFR in the presence of 1 pM to 100 pM mouse Egfr which shares 90% sequence identity with the human protein. The presence of a one-million-fold excess of mouse Egfr did not appear to interfere significantly with the quantification of human EGFR levels, as the LOD remained well below 100 aM and the assay background showed only a small increase (**Supplementary Fig. S1**), indicating the robust specificity of NULISA.

To demonstrate the sensitivity and accuracy of NULISA for the detection of biologically important, low-abundance proteins in complex samples, we investigated assay sensitivity, reproducibility, detectability, spike recovery, dilutional linearity, and parallelism in detecting neurofilament light protein (NfL), IL1B, and IL6 in plasma samples. All assays showed excellent detection sensitivity, 100% detectability in plasma samples, and acceptable accuracy (70-130%) in spike recovery, dilutional linearity, and parallelism tests (**Supplemental Fig. S2a-c**).

Collectively, these results demonstrated that the background suppression mechanisms in NULISA contributed to achieving attomolar-level sensitivity, and the qPCR-based NULISA outperformed the current state-of-the-art in sensitivity and dynamic range, and could detect and quantify low-abundance biomarkers in complex matrices with high sensitivity and accuracy.

NULISAseq enables highly multiplexed analysis with attomolar sensitivity

We next aimed to demonstrate NULISA's capacity to multiplex with NGS (NULISAseq). We developed a 200-plex inflammation panel that includes mostly cytokines, chemokines, and other inflammation/immunology-related targets, many of which are present at very low levels in the blood[5] (**Supplementary Data A**).

To first evaluate the sensitivity of the 200-plex NULISAseq assay, standard curves were generated using pooled recombinant proteins, and LODs were determined (**Supplemental Data A**). For comparison, single-plex standard curves for 11 targets were also constructed using individual recombinant proteins and qPCR-based NULISA using the same antibody reagents. Single-plex and multiplex assays demonstrated similar attomolar-level LODs: 58 aM and 37 aM for LIF, 20 aM and 7 aM for IL5, and 66 aM and 75 aM for IL13, respectively (**Fig. 2a**), indicating that high multiplexing was achieved in NULISAseq without a reduction in sensitivity. Furthermore, the results of the single-plex and 200-plex assays demonstrated excellent correlation for these targets in the 12 donor samples (Pearson correlation $r > 0.8$) (**Fig. 2b**). To further confirm that the design of NULISAseq allows flexible multiplexing with consistent results, we pooled 24 individual

assays from the 200-plex assay to create a 24-plex panel and used it to analyze the same 12 donor samples. The correlation between the results of the 200-plex and 24-plex NULISAseq methods was high ($r > 0.9$) for all targets (**Fig. 2c**).

Collectively, these results indicate that NULISAseq can multiplex >200 targets with similar sensitivity as qPCR-based single-plex, and the results from different levels of multiplexing are highly consistent.

Dynamic range, precision, cross-reactivity, and sample detectability

The 12-log dynamic range of plasma protein concentrations[5] poses a special challenge for multiplexing with NGS as the readout, because the total number of sequencing reads is constrained in each run and is dominated by high-abundance targets, reducing the probability of detecting reads from low-abundance targets. To simultaneously detect both high- and low-abundance targets, a relatively even distribution of sequencing reads across all targets is needed. To achieve this goal, we used a signal-tuning strategy, mixing unconjugated "cold" antibodies with DNA-conjugated "hot" antibodies at different ratios based on the endogenous levels of plasma proteins. The tuned signal from the hot/cold antibody mixture was proportional to the percentage of "hot" antibodies, while the shape of the standard curve was well maintained (**Supplementary Fig. S3**), indicating that signals or assay sensitivity for high-abundance proteins could be tuned down while maintaining detectability and quantifiability. Incorporating this strategy in the NULISAseq 200-plex, we determined the dynamic range of each assay using serial dilutions of the recombinant protein mix. Most assays showed a dynamic range greater than three logs, covering at least two logs above and one log below the endogenous levels in healthy donors (**Fig. 3a, Supplementary Data A**). The total dynamic range across all targets spanned close to 10 logs of plasma protein concentrations (**Fig. 3a**). The dynamic range could potentially be further expanded by deeper sequencing.

We next determined the precision of the NULISAseq 200plex assay. The intraplate CV was determined using 9 replicates each of 10 individual healthy donor samples. The intraplate CV was averaged across seven runs for each target. After normalization with

the internal control mCherry, the mean and median intraplate CVs across the targets were 10.2% and 9.2%, respectively. The interplate CV was determined using two runs with the same operator, instrument, and reagent lot, and after intensity normalization, the mean and median interplate CVs were calculated to be 10.3% and 9.1%, respectively (Fig. 3b, Supplementary Data A). Taken together, these results indicated that NULISAseq with the built-in intraplate and interpolate controls could generate data with high precision from well to well and plate to plate.

To assess potential cross-reactivity of the 200-plex assay, we randomly assigned 198 targets for which recombinant proteins were available to one of 45 pools of four or five targets each. We then repeated the random assignment to a second set of 45 pools such that no targets shared pools in both sets. We also included three additional pools of recombinant proteins that were not included in the 200-plex assay to further test cross reactivity to homologous proteins (**Supplementary Table S1**); in this experiment, one pool included proteins with >70% homology to any of the 200 analytes, and the other two pools contained proteins that are at least 50% homologous to two specific analytes, CEACAM5 and IFNA1. For most assays, only the pools containing the two assigned antigens generated a specific signal as expected, whereas other pools generated background-level reads for targets not included in the pool (**Fig. 3c**). Overall, 91% of the assays showed >99% specificity relative to the highest cross-reaction signal in the nontarget antigen pools (**Supplementary Data A**). The remaining assays with potential cross-reactions were further assessed using low- or single-plex assays. Two events of cross-reaction (IL4 and FGF23) were later identified as being due to antigen contamination originating from vendors, and the specificity calculated using uncontaminated antigens from a different source passed the >99% cut-off (**Supplementary Data A**). A few cross-reaction events were confirmed by pairwise studies, although their severity was lower than that estimated in the initial experiment (**Supplementary Data A**).

To assess target detectability in clinical samples, defined as the percentage of samples in which a target signal was detected above the LOD, we performed NULISAseq on 151

samples from 79 healthy donors and 72 patients with different diseases (Sample Sets 1 and 2; **Supplementary Tables S2 and S3**). The mean detectability across the 204 targets was 93.7%, 94.8%, and 94.4% in healthy, diseased, and combined samples, respectively, and overall, 195 (95.6%) targets demonstrated >50% detectability (percentage of samples detected above the LOD) (**Fig. 3e**, **Supplemental Data A**).

Collectively, these results indicated that the NULISAseq 200plex assay exhibited a wide dynamic range, excellent precision, and high target detectability in clinical samples.

NULISAseq comparison with other immunoassays

Having demonstrated the analytical performance parameters, we next compared the performance of NULISAseq with that of two commercial multiplex assays, the Olink Explore 384 Inflammation Panel and MSD V-PLEX Human Cytokine 44-Plex (which includes five separate 7- to 10-plex assays). Target detectability and inter-platform correlations were determined in a set of samples, including plasma samples from 39 healthy donors and 35 patients with different diseases (Sample Set 1 in **Supplementary Table S2**). NULISAseq demonstrated equal or better detectability than the other two assays for 20 of the 23 targets shared among the three assay platforms (**Fig. 4a**). The pairwise-correlations of the three platforms were high (NULISA vs. MSD mean r=0.76, median r=0.90; NULISA vs. Olink mean r=0.71, median r=0.84; MSD vs. Olink mean r=0.78, median r=0.87), especially for targets that showed good detectability across all three platforms (**Fig. 4a**). When detectability differed, the correlation was lower; for example, for IL5, NULISA and MSD both had high detectability (100% and 82.4%, respectively), and the results correlated well (r=0.76, p<0.001), but the results obtained from these two assays correlated poorly with those obtained from Olink (NULISA r=0.08, p=0.50; MSD r=0.11, p=0.41), which had poor detectability (24.3%). The results of the NULISA CCL3 assay showed poor correlation with those of the other two platforms because of low detectability.

We next compared NULISAseq and Olink Explore using 151 samples (Sample Sets 1 and 2) including two pooled healthy donor plasma samples with four replicates each on

each plate to evaluate assay precision. For the 92 common targets in the two panels, the mean and median intraplate CVs were comparable between NULISAseq (mean=7.3%, median=6.7%) and Olink (mean=8.4%, median=6.4%), with NULISAseq showing a narrower CV distribution (**Fig. 4b**). A similar pattern was observed for the interplate CV after intensity normalization (NULISAseq mean=11.6%, median=11.1%; Olink mean=12.5%, median=9.9%). The percentage of detectable targets for both panels exceeded 90% (96.7% for NULISAseq and 92.4% for Olink); however, NULISAseq showed better detectability in samples from both healthy individuals and patients (**Supplementary Table S4**). Assays showing the largest detectability differences between NULISAseq and Olink were those for low-abundance targets, such as IL4, IL5, IL11, IL13, IL20, IL33, and IL2RB (**Supplementary Fig. S4**). Taken together, NULISAseq demonstrated high precision and superior sensitivity for low abundance targets compared to existing immunoassays.

To assess whether the higher sensitivity of NULISAseq leads to better detection of low-abundance targets in differential expression analysis, we used linear models to identify differentially expressed targets between patients with inflammatory diseases or cancer and healthy controls. We compared the results for the 92 common targets with those obtained from Olink using a 5% false discovery rate (FDR) significance threshold. In the comparison of patients with inflammatory diseases (n=21) and healthy donors (n=79), NULISAseq and Olink identified 54 and 43 significantly different targets, respectively, 36 of which were identified using both platforms (**Fig. 4c**), again demonstrating high concordance between platforms. The correlation between the estimated abundance differences between the two platforms was also good ($r=0.67$, $p < 0.001$) (**Fig. 4d**). The largest differences in detectability were observed in some of the low-abundance targets that were poorly detected by the Olink assay (IL4, IL5, IL20, IL17A, IL17F, IL33, and IL2RB) (**Fig. 4e**). IL4 levels were elevated in all four groups of patients with autoimmune diseases (rheumatoid arthritis, Sjögren's syndrome, systemic lupus erythematosus and ulcerative colitis) (**Supplemental Fig. S6**), consistent with the role of this protein in B-cell hyperactivity, which mediates a broad spectrum of autoimmune diseases[22]. IL17A and IL17F are cytokines secreted by T helper 17 cells that play crucial roles in the

development of many autoimmune diseases[23]. IL33 levels are elevated in patients with autoimmune diseases, and IL33 is a potential therapeutic target[24]. These results indicate that the higher sensitivity of NULISAseq enables the identification of clinically important but low-abundance biomarkers.

In the comparison between cancer (n=32) and healthy donors (n=79), NULISAseq and Olink identified 20 and 27 significant targets, respectively, with 16 in common (**Supplemental Fig. S5a**), and the estimated differential expression showed good correlation between the two platforms ($r=0.70$, $p < 0.001$) (**Supplemental Fig. S5b**). The different numbers of significant targets between these two assays were not due to detection sensitivity differences since, except for FLT3LG, 10 of the 11 significant targets identified by Olink were highly detected by both platforms. This discrepancy might be due to the statistical instability associated with the small sample size (n=35) of a highly heterogeneous group of cancers (12 types) analyzed (**Supplemental Table S2**).

Characterization of the host response to SARS-CoV-2 infection with NULISAseq

COVID-19, caused by SARS-CoV-2, is characterized by the uncontrolled production of many cytokines and chemokines involved in innate and adaptive immune responses, resulting in systemic inflammation and tissue injury[25,26]. To elucidate the pathogenesis of COVID-19 and identify molecular markers that can be used to predict disease progression and prognosis, many groups have performed cytokine/immune profiling using different panels and technologies[26–31]. With the improved sensitivity of NULISAseq over other methods and the broad coverage of 124 cytokines and chemokines and 40 receptor molecules in the 200-plex Inflammation Panel, we next sought to characterize the host response to SARS-CoV-2 infection in patients with a mild COVID-19 disease course. The higher sensitivity of this method may represent a unique advantage in detecting mild COVID-19 because more subtle differences might be expected than in severe cases. In this experiment, we analyzed 51 serum samples from 11 patients with mild COVID-19 and 16 control samples from healthy donors based on a cohort previously studied for the development of anti-spike antibodies[32] (**Supplementary Table S5**). Because of the uncertainty of the exact onset of infection, the multiple timepoints from different individuals

were synchronized by setting the timepoint with peak expression of SARS-CoV-2 nucleocapsid protein (N-protein) as t_0 (n=11), as described previously[32]. Time points 2–7 days before t_0 were classified as t_{-1} (n=11), 2-7 days after t_0 as t_1 (n=14), and 8–20 days after t_0 as t_2 (n=15).

The resulting NULISA data were analyzed for differential abundance between samples obtained from COVID-19 patients at each time point group and the 16 control samples using a linear mixed model with age and sex as covariates and accounting for repeated measures[33]. This analysis identified a total of 80 significantly different targets (FDR-adjusted $p < 0.05$ per timepoint; 75 with elevated levels and 5 with decreased levels in mild COVID-19 patients; **Supplemental Data C**). Among these targets, a group of interferons, including type I interferons (IFNA1, IFNA2, IFNW1) and type III interferon IFNL1, exhibited large (9- to 400-fold) and coordinated increases in abundance across the first three timepoints (targets indicated by * in **Fig. 5a; Fig. 5b**), indicating a robust and sustained interferon response characteristic for anti-viral immune responses[34]. Two other interferons, IFNB1 (type I) and IFNG (type II), were also among the top 20 most differentially expressed targets (**Fig. 5b**). Interferons are normally present at very low concentrations in the blood (low pg/mL, https://proteinatlas.org) and thus present a challenge for detection. However, NULISAseq detected these proteins with high detectability in this cohort, including in the healthy controls, as follows: IFNA1 (100%), IFNA2 (69%), IFNB1 (100%), IFNW1 (78%), IFNG (100%), and IFNL1 (100%). A previous study using Olink PEA technology also detected elevated levels of IFNG and IFNL1 in COVID-19 patients, but the detection rates were lower at 76% for IFNG and 19% for IFNL1 [29].

The top 20 targets also included CXCL10 (IP-10), IL6 and IL10, a cytokine-chemokine triad associated with severe COVID-19[27], as well as C1QA, an important component of the complement system previously shown to be present at elevated levels in SARS-CoV-2-infected patients[35]. The 80 significantly different targets also included 11 (CCL16, CCL7, CXCL10, CCL8, IL1RN, CD274, IL6, IL18, MERTK, IFNG, and IL18R1, indicated with ** in **Fig. 5a**) of the 14 proteins detected in COVID-19 patients in multiple previous

studies[31], 13 of which were included in the 200-plex NULISA panel, although most of the patients in these prior studies had more severe disease[29]. Gene ontology (GO)[36] analysis of the 75 targets with elevated levels was performed. The results indicated enrichment in natural killer cell activation (GO:0030101), which has been reported elsewhere[37], regulation of lymphocyte differentiation (GO:0045619) and adaptive immune response (GO:0002250) (**Supplemental Data C**), indicating the activation of both innate and adaptive immune response mechanisms in response to SARS-CoV-2 infection. Taken together, these results indicated that NULISAseq was able to detect important low abundance proteins such as interferons and reveal many key aspects of the host response to SARS-CoV-2.

Conclusion

We developed NULISA to address the long-standing need for ultra-high sensitivity to detect low-abundance proteins in the blood proteome, as well as for high multiplexing to profile broad panels of proteins with high throughput and minimal sample usage. Our results demonstrate that NULISA achieves attomolar-level sensitivity, outperforms current ultrasensitive assays, and can measure hundreds of proteins simultaneously using 10-20 μl sample in a single reaction in a 96-well plate. NULISA's ultra-sensitivity stems from multiple mechanisms of background suppression. It adopts the PLA principle, which requires simultaneous binding of two antibodies to the target in proximity to generate a DNA reporter. NULISA reduces the assay background of traditional PLA by more than 10,000-fold by incorporating a unique molecular design of the DNA-antibody conjugate that enables sequential purification of the immunocomplexes on two solid surfaces prior to proximity ligation. With NULISAseq, high multiplexing was achieved by incorporating target- and sample-specific barcodes into the DNA reporter. In NULISAseq, sequencing identifies any remaining noncognate antibody-antibody interactions by matching target-specific barcodes in the DNA reporter to further reduce the background, which enables high levels of multiplexing while maintaining ultra-high sensitivity.

As the first application of this novel platform, we developed a 200-plex inflammation and immune response-focused panel including 124 cytokines and chemokines, as well as

other important inflammatory and immune-related proteins. To the best of our knowledge, this panel provides the highest coverage of cytokines and chemokines of any single inflammation-focused panel. The results of 200-plex NULISA demonstrated high concordance with those obtained from other immunoassays; moreover, NULISA can identify biologically important low-abundance biomarkers that are challenging to detect using other technologies, as demonstrated in our analysis of patients with inflammatory diseases and COVID-19, which is particularly noteworthy in the context of the current pandemic.

With improved sensitivity and broad coverage of cytokines and chemokines, the NULISA platform confirmed many key findings regarding the host response to SARS-CoV-2 infection, despite the limited sample size. In particular, we observed robust and sustained induction of all three types of interferons in patients with mild disease. Type I and type III interferons are the body's first-line defense against viral replication and spreading at the site of infection[38,39], but their detection in the blood requires ultra-high sensitivity[40]. One previous study was unable to detect circulating IFNB and IFNG in COVID-19 patient sera using traditional ELISA[41], and another study using the more sensitive SIMOA assay was able to detect IFNA in some patients but not in controls[27]. To our knowledge, the current study is the first to report the detection of IFNW1 in circulation and the detection of all three interferon types in a single assay. In fact, the different detection sensitivities of different assays used in various studies might have contributed to discrepant findings regarding the relationship between interferons and disease severity[40]. Some studies found a less pronounced interferon alpha response in patients with severe disease than in those with mild disease[41,42], another study reported persistently higher interferon alpha and lambda levels in patients with severe disease than in those with moderate disease[43], and yet another study found no association between interferon alpha levels and disease severity[28]. These findings highlight the critical importance of highly sensitive and robust assays in exploring the low-abundance portion of the proteome that is enriched in important cytokines, such as interferons and IL4[44].

NULISA generates the reporter DNA molecule by a simple ligation step, which makes multiplexing even easier with NULISA than with PEA, which requires predesigned sequence complementarity for hybridization between paired antibodies. This requirement makes it difficult to scale PEA beyond the 384-plex assay in a single reaction. We demonstrated the capacity of NULISA to achieve multiplexed detection of >200 targets, and we have shown >500-plex capability experimentally and designed >6,000 target-specific barcodes for much higher levels of multiplexing in the future.

The use of paramagnetic beads in NULISA also makes this protocol more amenable to automation by standard liquid handling equipment from commercial vendors, such as the TECAN and Hamilton instruments; for example, this study was performed using an in-house prototype system based on a Hamilton instrument. The automated protocol has a 6-hour run time and <30 min hands-on time from sample preparation to the acquisition of qPCR results or the preparation of a PCR-amplified DNA library ready for NGS sequencing. In comparison, Olink Explore is semi-automated requiring multiple different instruments and >5-hour hands-on time over two days. Automation not only increases sample throughput but also increases assay precision. Using our prototype system, the 200-plex assay demonstrated excellent precision with <10% median intraplate and interplate CVs.

The large dynamic range of protein concentrations in the blood plasma poses another challenge to multiplexing, especially when using NGS as a readout. Because each NGS run has a preset limit on the total number of sequencing reads, it is important to prevent high-abundance targets from generating too many reads to ensure that there is sufficient sequencing depth to detect and quantify low-abundance targets. To address this, the PEA protocol dilutes plasma samples to multiple levels and assigns groups of antibody probes to these dilution levels according to their target concentration ranges; this process adds complexity to sample handling and processing. In NULISA, we chose to tune down signals from high abundance targets by adjusting the ratio of “hot” and “cold” antibodies to equalize the distribution of reads across targets with different abundances. Using this approach, NULISA demonstrated a 9.6-log dynamic range with the 200-plex inflammation

panel. The ability to measure the levels of both high- and low-abundance proteins in the same reaction without sample dilution simplifies the creation of flexible panels from a large library of assays. We demonstrated this flexibility with consistent data generation across multiple protein abundance levels.

Currently, a dedicated system with tight integration of hardware, assay reagents, and software is in late-stage development. As the same instrument can be used to perform a flexible range of multiplexing with concordant results, it should greatly facilitate study designs to relieve the bottleneck in translation from discovery to validation.

In addition, as indicated by the low sensitivity of the NULISA CCL3 assay used in this study, antibody affinity and specificity still play an important role. Switching to a different antibody pair improved the sensitivity to 100% detectability (data not shown). Further efforts are needed to generate antibodies with high affinity and specificity in a predictable and scalable manner, which may be necessary for the analysis of many low-abundance biomarkers in demanding applications, such as early disease detection.

In conclusion, NULISA represents a major advance in sensitivity, multiplexing and ease of use in a proteomic platform. With unique content focusing on low abundance proteins in blood such as the cytokine/chemokine-rich 200-plex inflammation panel, NULISA has great potential for both biomarker discovery and validation, enabling novel liquid biopsy-based applications from early detection of diseases to informing prognosis, therapy selection and patient outcomes, and perhaps even leading to a deeper understanding of human biology at the system level.

Materials and Methods

Patients and samples

Human EDTA plasma samples from healthy donors and patients with various diseases (**Supplemental Table S2**) were purchased from BioIVT (Westbury, NY) and stored at -80 °C. Patient demographics and clinical diagnostic information (**Supplemental Table S3**) were provided by BioIVT.

The patients in the COVID-19 study were a subset of the mild disease cohort described previously[32]. In brief, samples were collected from January to March 2020 up to six times during the 21 days from inclusion in a study in Germany in the region of North Rhine-Westphalia. SARS-CoV-2 infection status was confirmed in all patients by qRT–PCR or antigen tests for SARS-CoV-2 using nasopharyngeal swabs and quantification of SARS-CoV-2 nucleocapsid (N) protein concentrations and serum anti-N Ab titers. Blood sampling of SARS-CoV-2-infected patients and healthy controls was approved by the local institutional research ethics board (University Hospital Bonn, ethics vote 468/20). We collected comprehensive clinical and demographic information, medical history, comorbidity information, and vaccination schedules for all patients and participants. This study was conducted in accordance with the principles of the Declaration of Helsinki.

Antibody-oligonucleotide conjugation and pooling of antibody conjugates

Antibody-oligonucleotide conjugation was performed based on amine-to-sulfhydryl cross-linking chemistry. For each target, capture and detection antibodies were conjugated to partially double-stranded DNA containing a polyA-containing oligonucleotide and a biotin-modified oligonucleotide, respectively. Antibody-oligonucleotide conjugates were purified to remove unreacted antibodies and oligonucleotides.

For each assay in the NULISAseq 200-plex inflammation panel, the “hot” DNA-antibody conjugate was mixed with nonconjugated “cold” antibodies at a ratio that was tuned to cover the range from ~10-fold below to ~100-fold above the baseline level in healthy donor plasma. The capture and detection antibodies for all targets in the 200plex assay were pooled.

NULISA and NULISAseq

NULISA reagents, including Assay Diluent (AD), Wash Buffer (WB), Elution Buffer 1 (EB1), oligo-dT paramagnetic beads (dT beads), streptavidin-coated paramagnetic beads (streptavidin beads), Elution Buffer 2 (EB2) and Ligation Master Mix (LMM), were developed by Alamar Biosciences. Plasma samples were briefly centrifuged at 10,000 × g for 10 min or filtered through a 1.2-μm filter plate (Millipore Sigma, Cat. No. MSBVN1210) prior to use. For single-plex NULISA, 10 or 20 μL of sample was added to a reaction mixture (total volume =100 μL) containing capture and detection antibody conjugates and AD buffer that included heterophilic blockers. For NULISAseq, 10 μL of sample was used in a 100 μL reaction containing capture and detection antibody cocktails in AD buffer. The reaction mixture was incubated at room temperature for one hour to allow the formation of immunocomplexes.

After immunocomplex formation, the following NULISA workflow was carried out automatically by a preprogrammed MicroLab STARlet liquid handler (Hamilton Company, Reno. NV), which was integrated with a KingFisher Presto magnetic bead processor (Thermo Fisher, Waltham, MA) and a BioTek ELx405 microplate washer (Agilent, Santa Clara, CA). In brief, 10 μL of dT beads was added to the reaction and incubated at room temperature for one hour, allowing capture of the immunocomplex on the bead surface. After washing with WB buffer, dT beads were transferred into EB1 buffer to release the immune complex from the bead surface. The eluate was then incubated with streptavidin beads for 5 min at room temperature to recapture the immunocomplex using the biotin-containing detection antibody conjugate. After additional washing with WB buffer, the SA beads were incubated with the ligation reagent LMM and a ligator sequence at room temperature for 10 min to generate the ligated reporter oligonucleotide. For single-plex NULISA the same ligator sequence was used for all samples. For NULISAseq, a ligator sequence containing a unique sample barcode was used for each sample analyzed. After ligation, reporter molecules were eluted from the SA beads using EB2 buffer for 10 min at room temperature. The final eluate was collected for quantification by qPCR for single-plex NULISA and by NGS for NULISAseq.

For qPCR analysis, 10 μL of the final eluted sample was added to a total of 30 μL containing PCR Master Mix (PMM, Alamar Biosciences). PCR samples were loaded onto a CFX96 Real-Time PCR instrument (Bio-Rad Laboratories, Hercules, CA, USA). The following PCR conditions were used: 30°C for 5 min; 95°C for 2 min; and 45 cycles of95°C for 3 s and 65°C for 30 s. The Cq values for each sample were acquired using the Bio-Rad Maestro software.

For NGS analysis, a library was prepared by pooling the reporter molecules from each NULISAseq reaction and then amplifying the products by 16 cycles of PCR. The library was cleaned using Ampure

XP reagent (Beckman Coulter), following the manufacturer's protocol. The library was then quantified using the Qubit 1X dsDNA HS assay kit (Thermo Fisher) before being loaded on a NextSeq 1000/2000 instrument (Illumina). For the NULISAseq 200-plex inflammation panel, a P2 reagent kit (100 cycles) (Illumina) was used for NGS.

Proximity ligation assay

The PLA reaction was set up in the same way as for single-plex NULISA. The immunocomplex formation step was performed by incubating the reaction at room temperature for 2 h, which is the same as the combined time for immunocomplex formation and dT bead capture steps in NULISA. After incubation, the reaction was diluted 100 times before the ligation step was performed under the same conditions as those used for NULISA. Ligation was terminated by heating at 75 ℃ for 15 minutes. Then, 10 μL of the final sample was used for qPCR analysis.

Cross-platform comparison

The Simoa® NfL and HIV p24 assays were performed by Frontage Laboratories (Exton, PA) using the Simoa® NF-light™ V2 Advantage kit (Quanterix, Billerica, MA) and Simoa® HIV p24 Advantage kit (Quanterix, Billerica, MA), respectively. For the correlation study with the NfL assay, 16 samples consisting of normal plasma, serum, plasma from patients with diseases, and CSF were tested using the SIMOA assay by Frontage Laboratories and internally tested with NULISA using a selected pair of antibodies that were different from those used in the SIMOA NfL assay. To compare the performance of the HIV p24 assay, a panel of 16 samples was created by spiking various levels of recombinant p24 into pooled normal plasma, which was then tested using both SIMOA (Frontage) and NULISA (internal) platforms.

Olink PEA was performed by Fulgent Genetics (Temple City, CA, USA) and the High-Throughput Biomarker Core of Vanderbilt University Medical Center (Nashville, TN, USA), both of which are designated Olink service providers. Seventy-two samples from patients with diagnosed diseases were grouped into broad diagnostic categories (**Supplementary Table S1**). Stratified sampling was used to randomize the assignment of 79 samples from healthy volunteers and 72 samples from patients with different diseases to each of the two plates (**Supplementary Table S2**). The same set of samples was profiled using the NULISAseq 200-plex Inflammation panel and the Olink Explore 384 Inflammation kit (Olink Proteomics, Uppsala, Sweden).

The V-PLEX Human Cytokine 44-Plex assay (Meso Scale Discovery (MSD), Rockville, MD, USA) was performed by DC3 Therapeutics (South San Francisco, CA, USA), a qualified MSD service provider, using five V-PLEX kits (Chemokine Panel 1, Cytokine Panel 1, Cytokine Panel 2, Proinflammatory Panel 1, and TH17 Panel 1). A subset of 39 samples from healthy volunteers and 35 samples from patients with different diseases from the above NULISAseq vs. Olink comparison study (**Supplementary Table S2**, Sample Set 1) was used to compare detectability and assess correlation for 23 common targets across the three platforms.

Data analysis

NULISAseq data processing and normalization

NGS data were processed using the NULISAseq algorithm (Alamar Biosciences). The sample (SMI) and target-specific (TMI) barcodes were quantified, and up to two mismatching bases or one indel and one mismatch were allowed. Intraplate normalization was performed by dividing the target counts for each sample well by the internal control (mCherry) counts. When multiple plates were analyzed together, interplate normalization was performed using interplate control (IPC) normalization or intensity normalization (IN). For IPC normalization, counts were divided by the target-specific medians of the three IPC wells on that plate. For IN, counts were divided by target-specific medians of all samples on a plate and then multiplied by global target-specific medians across all plates. For statistical testing, normalized counts were log2-transformed to form a more normal distribution.

Standard curve and LOD determination

For single-plex NULISA, Cq values were transformed ($2^{(37-Cq)}$) prior to 4PL curve fitting with $1/y^2$ error weighting. The LOD was calculated as 2.5 times the standard deviation of the measurements obtained from blank samples plus either the mean of the results from blanks or the y-intercept of the curve fit. These values were backfitted, and the maximum value was used to define the LOD in aM. To determine the LOD of NULISAseq in aM, normalized counts were fitted with a 4PL curve-fitting algorithm. This LOD was calculated as described above, but three times the standard deviation of the results obtained from the blanks was used.

Multiplex NULISAseq performance

200-plex, 24-plex, and single-plex NULISA correlations. Pearson correlations were calculated for each common target using the mean of two replicates each from 12 healthy donor samples. To ensure

more normally distributed data, correlations were assessed using log2-transformed absolute concentrations for single-plex and log2 normalized counts for NULISAseq.

Dynamic range. The dynamic range was determined for 197 NULISAseq targets using 12-point standard curves. The dynamic range interval was defined as the largest interval in which the coefficient of variation (CV) of all standards fell below 30% and the recovery was within 30%. A maximum of one standard, except for the lower and upper limit of quantitation (LLOQ and ULOQ), was allowed to fall outside the allowable recovery limits. LODs for each target in aM were determined as described above.

Precision. The intraplate CV was calculated using normalized counts for each of the 204 targets using nine replicates each of 10 healthy donor samples. The run was repeated seven times, and the target-specific mean intraplate CVs were calculated. Interplate CVs were calculated after intensity normalization for two of these runs, which used the same operator, instrument, antibody, and reagent lot. Results with values below the LOD were excluded from the CV calculations.

Cross-reactivity. To assess cross-reactivity, 198 targets were randomly assigned to two sets of 45 pools containing either four or five targets each, so that no two targets shared a pool for both sets. Counts were normalized using the internal control mCherry. The specificity for each target was quantified as 1 - (maximum non-target pool count – background)/(average target pool counts – background), where the background was calculated as the median count across all 90 pools.

NULISAseq versus Olink detectability and differential expression. Plate-specific LODs were determined for each of the 204 NULISAseq targets. The detectability for each target was calculated as the percentage of samples with results above the LOD, and a target was considered detectable when more than 50% of samples had results above the LOD. The same procedure was followed for Olink Explore data using LODs provided in the data output. For NULISAseq data, intraplate CVs were calculated based on normalized data for each target using two pooled plasma samples (four replicates each). Then target-wise mean CVs were calculated from the CVs of individual targets. The same procedure was followed for Olink data, but since data obtained from the Olink Explore unit NPX are on the $\log_2$ scale, intraplate CVs were calculated using the formula CV_j=100*\sqrt{e^(\sigma_j^2)-1}, where \sigma_j=sd(target_j NPX)*ln(2) as described[20]. Interplate CVs were calculated in a similar fashion for NULISAseq and Olink NPX data after applying intensity normalization. Results with values below the LOD were excluded from CV calculations for both platforms.

For the analysis of patients with inflammatory disease and cancer, differential expression relative to healthy controls was assessed using log2 intensity normalized data for the 92 shared NULISAseq and Olink targets using a linear regression model fitted separately for each target and adjusted for age, sex, plate, and disease status. The Benjamini-Hochberg FDR correction[45] was applied to the analysis of disease status across the 92 targets, and statistical significance was defined using a 5% FDR cutoff.

NULISAseq comparison with the Olink Explore 384 Inflammation Panel and MSD V-Plex Human Cytokine 44-Plex The detectability of the 23 common targets between the three assays was calculated as the percentage of samples with results above the LOD. Pearson correlation results were assessed on the log2 scale.

Characterization of the host response to SARS-CoV-2 infection with NULISAseq

Samples from each time point group were compared to healthy donor samples using mixed-effect linear models with age and sex as covariates and subject as a random effect using the limma R package[33]. Statistical significance was defined as an FDR-adjusted p-value < 0.05. Clustered heatmap visualization was performed using the ComplexHeatmap R package [46]. Both target and sample clustering were performed using cosine correlation distance and complete linkage.

Pathway analysis. Differentially expressed proteins were analyzed for pathway enrichment using the metascape web tool (https://metascape.org)[47]. The multiple gene list option was used to set the full 204 panel targets as background.

Software

All data analyses were performed using R software (v.4.2.0, R Core Team, 2021)[48].

Acknowledgement

We thank Alex Doe, Alex Lee, Angela Cifelli, Lucie Lee, and Yuanhui Huang for providing reagents for this study, Meirong Bai, Danielle Zhou, Roopa Comandur, and Angela Cifelli for assay development, Sydney Ho, Joseph Lau, and Tianyang Bai for antibody conjugation method development and production, April Falcone and Khaled Alganem for assistance with figures. Many thanks to the patients and their families who volunteered to donate blood. The authors express their gratitude to the University Hospital Bonn for providing infrastructure, and transportation possibilities during the phase of sample

collection. The authors thank Rolf von Uslar for interconnecting the project and the medical soldiers from the German Armed Forces.

Author Contributions

Y.L. conceived the NULISA concept, and led the project with X.M.. Y.L., W.F., Y.Y., A.G. and S.C. designed the NULISA system. Y.L., W.F., Y.Y. and X.M. designed the study. S.V.S., E.C., X.M. and Y.L. designed the COVID-19 study. X.M. wrote the manuscript with the help of J.B., Y.L., W.F., Y.Y., A.K., Q.H., D.K. and S.V.S.. Q.H., I.A., A.S., A.K., M.M., K.C., X.X. and S.I. performed the experiments. J.B., X.M., D.K. and K.B. performed the data analyses. D.W., J.B., and K.B. developed the bioinformatic pipelines. T.Y., R.N., L.W., M.Y., J.H., X.Q. and BQ performed assay development. K.E., J.H., L.Z., W.X. and L.F. performed reagent development and manufacturing. Y.Y., J.L. and C.H.P. developed the antibody conjugation protocol. S.C., K.Z. and C.P. built the automated assay system. S.V.S., A.O., J.S., and E.C collected the samples and patient data for the COVID-19 study.

Funding

This project was supported in part by the National Cancer Institute Small Business Innovation Research grant 1R43CA254548-01 to Y.L.. E.L. and S.V.S were supported by the Ministry for Science and Education of the Republic of Germany (COVIMMUNE/01KI20343, BMBF) and the German Research Foundation (DFG) projects: Excellence Cluster EXC 2151 (ID: 390873048) and IRTG2168 (ID: 272482170).

Bonn COVIMMUNE Consortium

Christoph Wilhelm, Christian Bode, Christian Putensen, Zeinab Abdullah, Natalio Garbi, Eicke Latz, Susanne Schmidt, Gunther Hartmann, Hendrik Streeck & Beate M. Kümmere

Competing interests

Patent applications on the NULISA technology described herein have been filed by Alamar Biosciences.

Additional information

Supplemental files (figures and data files) are listed in **List of Supplementary Materials.docx**, which also contains Supplemental Tables.

References

1. Hartwell, L., Mankoff, D., Paulovich, A., Ramsey, S. & Swisher, E. Cancer biomarkers: a systems approach. *Nature Biotechnology 2006 24:8* **24**, 905–908 (2006).
2. Dodgson, S. E. There Will Be Blood Tests. *Cell* **173**, 1–3 (2018).
3. Nikanjam, M., Kato, S. & Kurzrock, R. Liquid biopsy: current technology and clinical applications. *J Hematol Oncol* **15**, (2022).
4. Cescon, D. W., Bratman, S. v., Chan, S. M. & Siu, L. L. Circulating tumor DNA and liquid biopsy in oncology. *Nat Cancer* **1**, 276–290 (2020).
5. Anderson, N. L. & Anderson, N. G. The Human Plasma Proteome: History, Character, and Diagnostic Prospects *. *Molecular & Cellular Proteomics* **1**, 845–867 (2002).
6. Uhlén, M. *et al.* The human secretome. *Sci Signal* **12**, eaaz0274 (2019).
7. Williams, S. A. *et al.* Plasma protein patterns as comprehensive indicators of health. *Nat Med* **25**, 1851–1857 (2019).
8. Melani, R. D. *et al. The Blood Proteoform Atlas: A reference map of proteoforms in human hematopoietic cells*. https://www.science.org.
9. Wishart, D. S. *et al.* MarkerDB: an online database of molecular biomarkers. *Nucleic Acids Res* **49**, D1259–D1267 (2021).
10. Aebersold, R. & Mann, M. Mass spectrometry-based proteomics. *Nature 2003 422:6928* **422**, 198–207 (2003).
11. Ren, A. H., Diamandis, E. P. & Kulasingam, V. Uncovering the Depths of the Human Proteome: Antibody-based Technologies for Ultrasensitive Multiplexed Protein Detection and Quantification. *Molecular & Cellular Proteomics* **20**, 100155 (2021).
12. Niemeyer, C. M., Adler, M. & Wacker, R. Immuno-PCR: high sensitivity detection of proteins by nucleic acid amplification. *Trends Biotechnol* **23**, 208–216 (2005).
13. Fredriksson, S. *et al.* Protein detection using proximity-dependent DNA ligation assays. *Nat Biotechnol* **20**, 473–477 (2002).
14. Darmanis, S. *et al.* ProteinSeq: high-performance proteomic analyses by proximity ligation and next generation sequencing. *PLoS One* **6**, (2011).
15. Lundberg, M., Eriksson, A., Tran, B., Assarsson, E. & Fredriksson, S. Homogeneous antibody-based proximity extension assays provide sensitive and specific detection of low-abundant proteins in human blood. *Nucleic Acids Res* **39**, e102–e102 (2011).
16. Rissin, D. M. *et al.* Simultaneous detection of single molecules and singulated ensembles of molecules enables immunoassays with broad dynamic range. *Anal Chem* **83**, 2279–2285 (2011).
17. Hwang, J. *et al.* Quantitation of low abundant soluble biomarkers using high sensitivity Single Molecule Counting technology. *Methods* **158**, 69–76 (2019).
18. Kellar, K. L., Mahmutovic, A. J. & Bandyopadhyay, K. Multiplexed microsphere-based flow cytometric immunoassays. *Curr Protoc Cytom* **Chapter 13**, (2006).
19. Candia, J., Daya, G. N., Tanaka, T., Ferrucci, L. & Walker, K. A. Assessment of variability in the plasma 7k SomaScan proteomics assay. *Scientific Reports* | **12**, 17147 (123AD).
20. Wik, L. *et al.* Introducing a new era in proteomics - Proximity Extension Assay in combination with Next Generation Sequencing for high-throughput proteome-wide analysis. *Molecular & Cellular Proteomics* **20**, 100168 (2021).

21. Wang, F. *et al.* RNAscope: a novel in situ RNA analysis platform for formalin-fixed, paraffin-embedded tissues. *J Mol Diagn* **14**, 22–29 (2012).
22. Hui, C. W., Wu, W. C. & Leung, S. O. Interleukins 4 and 21 Protect Anti-IgM Induced Cell Death in Ramos B Cells: Implication for Autoimmune Diseases. *Front Immunol* **13**, 919854 (2022).
23. Tabarkiewicz, J., Pogoda, K., Karczmarczyk, A., Pozarowski, P. & Giannopoulos, K. The Role of IL-17 and Th17 Lymphocytes in Autoimmune Diseases. *Archivum Immunologiae et Therapiae Experimentalis 2015 63:6* **63**, 435–449 (2015).
24. Theoharides, T. C., Petra, A. I., Taracanova, A., Panagiotidou, S. & Conti, P. Targeting IL-33 in Autoimmunity and Inflammation. *Journal of Pharmacology and Experimental Therapeutics* **354**, 24–31 (2015).
25. Mangalmurti, N. & Hunter, C. A. Cytokine Storms: Understanding COVID-19. *Immunity* **53**, 19–25 (2020).
26. Costela-Ruiz, V. J., Illescas-Montes, R., Puerta-Puerta, J. M., Ruiz, C. & Melguizo-Rodríguez, L. SARS-CoV-2 infection: The role of cytokines in COVID-19 disease. *Cytokine Growth Factor Rev* **54**, 62–75 (2020).
27. Laing, A. G. *et al.* A dynamic COVID-19 immune signature includes associations with poor prognosis. *Nat Med* **26**, 1623–1635 (2020).
28. Thwaites, R. S. *et al.* Inflammatory profiles across the spectrum of disease reveal a distinct role for GM-CSF in severe COVID-19. *Sci Immunol* **6**, (2021).
29. Filbin, M. R. *et al.* Longitudinal proteomic analysis of severe COVID-19 reveals survival-associated signatures, tissue-specific cell death, and cell-cell interactions. *Cell Rep Med* **2**, (2021).
30. Ling, L. *et al.* Longitudinal Cytokine Profile in Patients With Mild to Critical COVID-19. *Front Immunol* **12**, 4984 (2021).
31. Suhre, K. *et al.* Identification of Robust Protein Associations With COVID-19 Disease Based on Five Clinical Studies. *Front Immunol* **12**, 781100 (2022).
32. Odainic, A. *et al.* Comparative Analysis of Antibody Titers against the Spike Protein of SARS-CoV-2 Variants in Infected Patient Cohorts and Diverse Vaccination Regimes. *Int J Mol Sci* **23**, (2022).
33. Ritchie, M. E. *et al.* limma powers differential expression analyses for RNA-sequencing and microarray studies. *Nucleic Acids Res* **43**, (2015).
34. Katze, M. G., He, Y. & Gale, M. Viruses and interferon: a fight for supremacy. *Nature Reviews Immunology 2002 2:9* **2**, 675–687 (2002).
35. Stephenson, E. *et al.* Single-cell multi-omics analysis of the immune response in COVID-19. *Nature Medicine 2021 27:5* **27**, 904–916 (2021).
36. Carbon, S. *et al.* The Gene Ontology resource: enriching a GOld mine. *Nucleic Acids Res* **49**, D325–D334 (2021).
37. Zafarani, A. *et al.* Natural killer cells in COVID-19: from infection, to vaccination and therapy. *Future Virol* (2023) doi:10.2217/FVL-2022-0040.
38. Lazear, H. M., Schoggins, J. W. & Diamond, M. S. Shared and Distinct Functions of Type I and Type III Interferons. *Immunity* **50**, 907–923 (2019).
39. Sposito, B. *et al.* The interferon landscape along the respiratory tract impacts the severity of COVID-19. *Cell* **184**, 4953-4968.e16 (2021).
40. Smith, N. *et al.* Defective activation and regulation of type I interferon immunity is associated with increasing COVID-19 severity. *Nat Commun* **13**, (2022).

41. Hadjadj, J. *et al.* Impaired type I interferon activity and inflammatory responses in severe COVID-19 patients. *Science (1979)* **369**, 718–724 (2020).
42. Blanco-Melo, D. *et al.* Imbalanced Host Response to SARS-CoV-2 Drives Development of COVID-19. *Cell* **181**, 1036-1045.e9 (2020).
43. Lucas, C. *et al.* Longitudinal analyses reveal immunological misfiring in severe COVID-19. *Nature 2020 584:7821* **584**, 463–469 (2020).
44. Huan, X. *et al.* Increased serum IL-2, IL-4, IL-5 and IL-12p70 levels in AChR subtype generalized myasthenia gravis. *BMC Immunol* **23**, (2022).
45. Benjamini, Y. & Hochberg, Y. Controlling the False Discovery Rate: A Practical and Powerful Approach to Multiple Testing. *Journal of the Royal Statistical Society: Series B (Methodological)* **57**, 289–300 (1995).
46. Gu, Z., Eils, R. & Schlesner, M. Complex heatmaps reveal patterns and correlations in multidimensional genomic data. *Bioinformatics* **32**, 2847–2849 (2016).
47. Zhou, Y. *et al.* Metascape provides a biologist-oriented resource for the analysis of systems-level datasets. *Nat Commun* **10**, 1523 (2019).
48. R Development Core Team. R: A Language and Environment for Statistical Computing. Preprint at http://www.r-project.org/ (2010).

Figure Legends

Fig. 1 | NULISA design and proof of concept. a. Schematic of the NULISA workflow. 1) Immunocomplex formation; 2) first capture of immunocomplexes to dT beads; 3) bead washing to remove unbound antibodies and sample matrix components; 4) release of immunocomplexes into solution; 5) recapture of immunocomplexes onto streptavidin beads; 6) bead washing and DNA strand ligation to generate reporter DNA; 7a) detection and quantification of reporter DNA levels by qPCR; 7b) quantification of reporter DNA levels by NGS. **b**. Standard curves for IL4 detection generated following the traditional PLA or NULISA protocols using the same set of reagents. **c**. Sensitivity and dynamic range comparison between NULISA and SIMOA using the same pair of antibodies.

Fig. 2 | NULISAseq sensitivity and correlation across multiplex levels. a. Comparison of the sensitivity of 200-plex and single-plex assays for LIF, IL5, and IL13 detection. **b.** Pearson correlation of protein levels measured using 200-plex and single-plex assays with 12 individual healthy donor plasma samples. The 200-plex data were first normalized using an internal control and then log2-transformed. Single-plex data in absolute concentration (aM) were also log2-transformed. Least-squares regression lines

are shown on the plots. **c.** Pearson correlation of protein levels measured using 200-plex and 24-plex NULISA methods with the same 12 plasma samples. Data were first normalized using an internal control and then log2-transformed. Least-squares regression lines are shown on the plots. The same antibody concentrations were used in all the assays.

Fig. 3 | NULISAseq performance characterization. a. The dynamic range for the detection of each target is indicated by the dark blue region. Values above the limit of detection (LOD) but below the lower limit of quantitation (LLoQ) are shown in lighter blue. Targets are ordered according to the geometric mean of the LLoQ and upper limit of quantitation (ULoQ). Dark blue lines represent generalized additive model (GAM) cubic regression spline fits to the ULoQ and LLoQ. The overall dynamic range for 200-plex NULISAseq spanned 9.6 log values. **b**. Density plots of intraplate CV after internal control normalization (**top**) and interplate CV after internal control and intensity normalization (**bottom**). **c**. Cross reactivity. Two sets of 45 random antigen pools containing 4-5 targets each were analyzed with 200-plex NULISAseq. Each cell of the heatmap represents the percent of normalized read counts for that target (rows) occurring in that pool (columns). Targets were ordered according to pool membership such that the cells on the diagonal corresponded to the assigned pools. **d**. Detectability of 204 targets in 151 samples, including 79 from healthy controls and 21 from patients with various diseases.

Fig. 4 | Comparison of NULISAseq with other assay platforms. a. Detectability and interplatform correlations for 23 shared targets in the NULISAseq 200-plex, Olink Explore 384 Inflammation Panel, and MSD V-PLEX Human Cytokine 44-Plex assays. Interplatform correlations were higher for more detectable targets. **b**. Intra- and interplate CV distributions for the 92 common targets in the NULISAseq 200-plex and Olink Explore 384 Inflammation Panel. **c**. Differential expression analysis comparing 21 samples from patients with inflammatory disease and 79 samples from healthy controls using the 92 shared targets between NULISAseq and Olink Explore. Volcano plot of -log10(FDR-adjusted p-value) versus log2(fold change) levels detected using

NULISAseq (**left**) and Olink Explore (**middle**). **Right**, Venn diagram showing the overlap of significantly different targets between the two assays. **d**. Correlation of estimated log2-fold changes between NULISAseq and Olink Explore. Targets detected by one platform but not the other are highlighted in blue (detected by NULISAseq only) or red (detected by Olink only). Targets in black were detected by both panels, and targets in grey were not significant for either panel. **e**. Comparison of detectability between NULISAseq and Olink Explore. Targets detected by one platform but not the other are highlighted in blue (detected by NULISAseq only) or red (detected by Olink only); other targets are in black.

Fig. 5 | Heatmap of differentially expressed targets between SARS-CoV-2-infected patients and healthy controls by day. Linear mixed effect model differential expression analysis between 11 mild COVID-19 patients within each time period (some individuals had repeated measurements within a given time period) and 16 healthy donor samples identified a total of 80 significantly different targets. Significantly different targets were visualized in a clustered heatmap showing the targets in rows and samples in columns. The heatmap displays the log2-normalized read counts centered relative to the mean in the healthy control samples. Both target and sample clustering were performed using cosine correlation distance and complete linkage. Target names provided in the text are marked with asterisks: * indicates interferons, and ** indicates 14 targets previously reported to be associated with COVID-19[31]. Time T_0 (n=11) represents peak expression of SARS-CoV-2 nucleocapsid protein (N-protein); time T-7 to -2 (n=11) represents 2 to 7 days before T_0, T2 to 7 represents 2 to 7 days after T_0 (n=14), and T8 to 20 represents 8 to 20 days after T_0 (n=15). **b,** Individual trajectories of interferon expression relative to days from peak N-protein are shown for the mild COVID group (gold lines). Trajectories are aligned based on the day of peak N-protein (dashed gray vertical line). Generalized additive models with a cubic regression spline basis were used to estimate the mean mild COVID-19 trajectory (dark brown line). Control samples (lighter blue open circles) and control group mean (dark blue solid circle) are shown to the left.

Figure 1

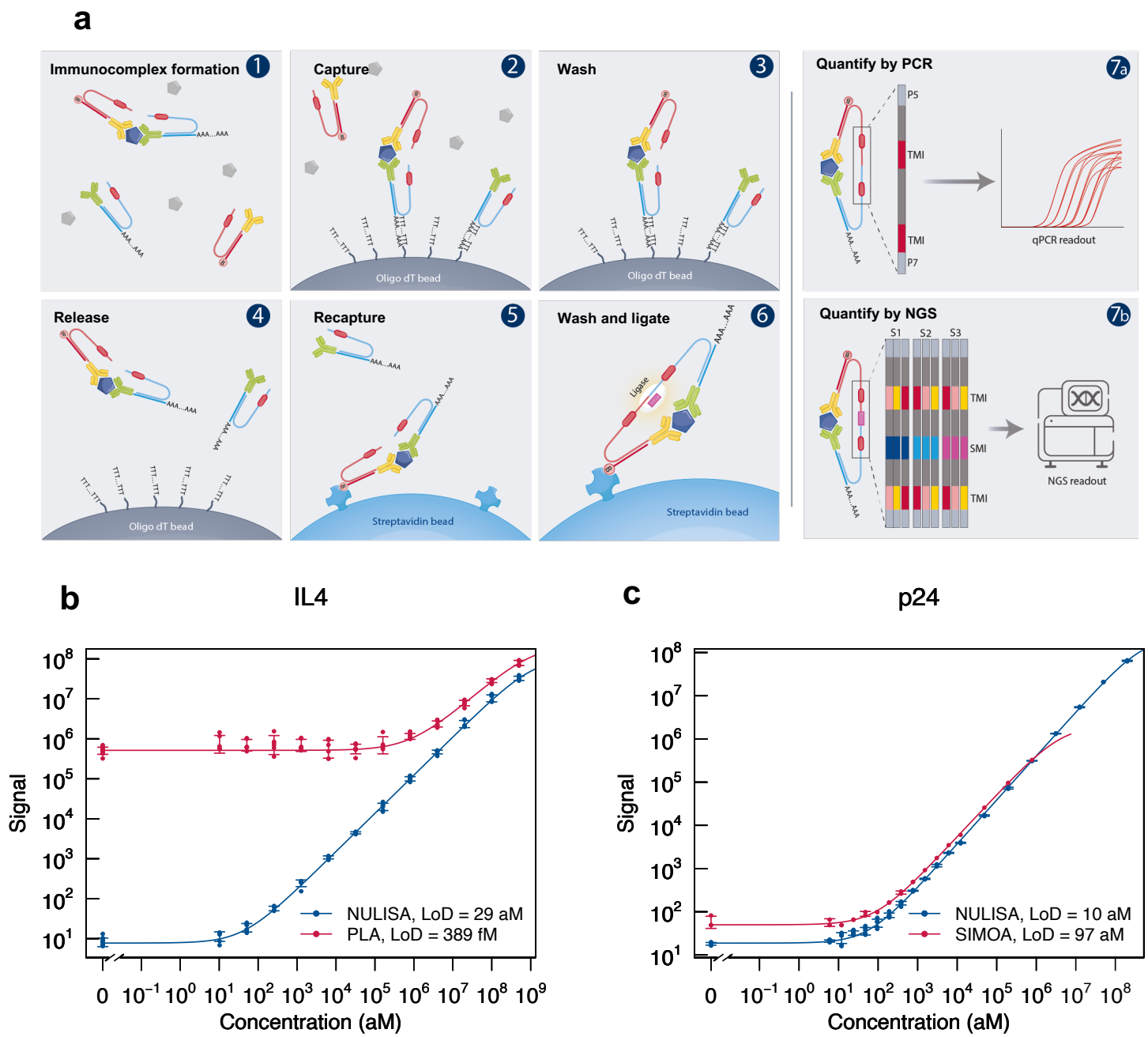
a
Immunocomplex formation
1
Capture
2
Wash
3
Quantify by PCR
7a
Release
4
Recapture
5
Wash and ligate
6
Quantify by NGS
7b
Oligo dT bead
Streptavidin bead
Ligase
P5
TMI
P7
qPCR readout
S1
S2
S3
SMI
NGS readout
b
IL4
Signal
Concentration (aM)
NULISA, LoD = 29 aM
PLA, LoD = 389 fM
c
p24
Signal
Concentration (aM)
NULISA, LoD = 10 aM
SIMOA, LoD = 97 aM

Figure 2

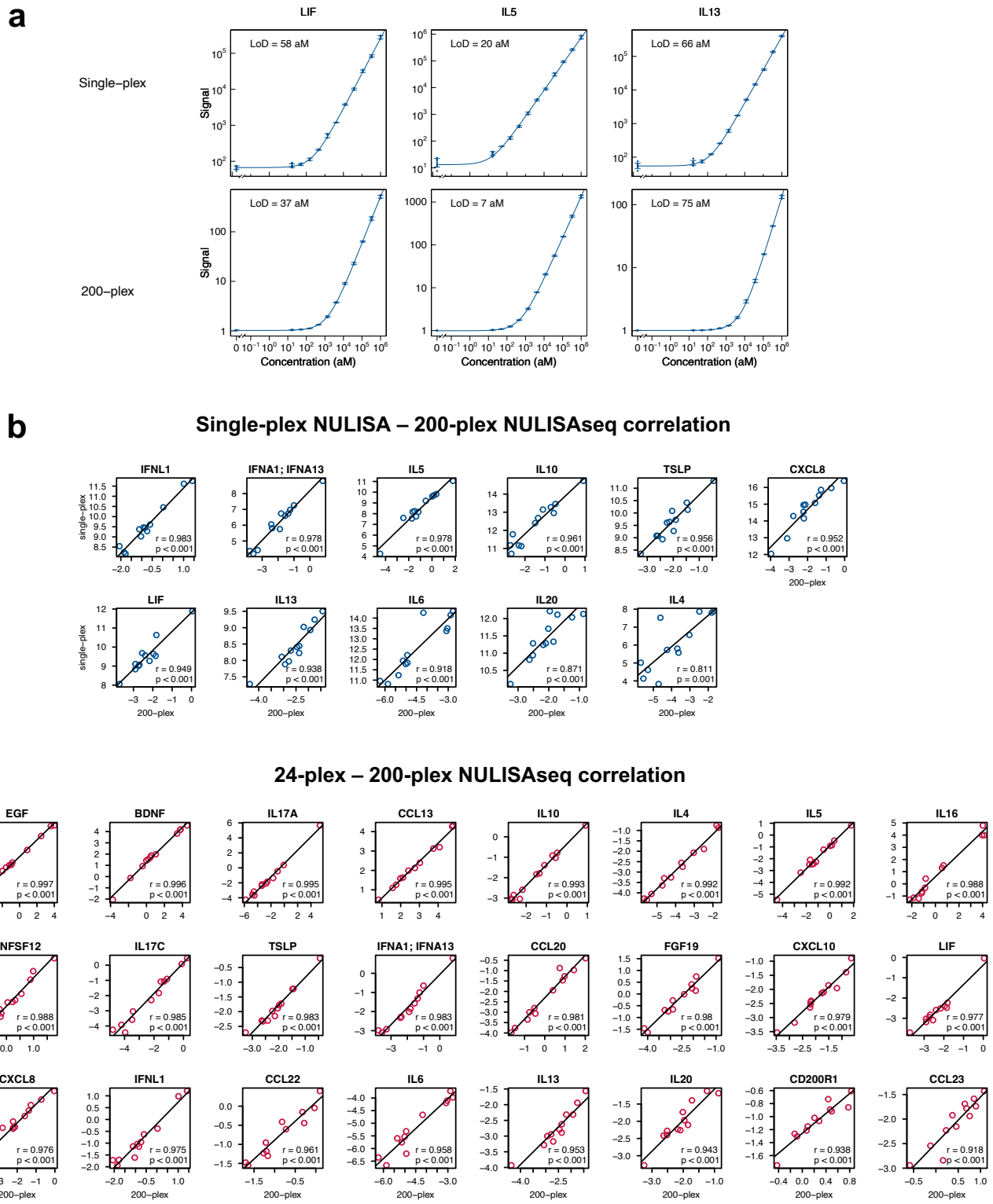
a
LIF
IL5
IL13
Single−plex
200−plex
Signal
LoD = 58 aM
LoD = 20 aM
LoD = 66 aM
LoD = 37 aM
LoD = 7 aM
LoD = 75 aM
Concentration (aM)
b
Single-plex NULISA – 200-plex NULISAseq correlation
IFNL1
IFNA1; IFNA13
IL5
IL10
TSLP
CXCL8
LIF
IL13
IL6
IL20
IL4
single−plex
200−plex
r = 0.983
p < 0.001
r = 0.978
p < 0.001
r = 0.978
p < 0.001
r = 0.961
p < 0.001
r = 0.956
p < 0.001
r = 0.952
p < 0.001
r = 0.949
p < 0.001
r = 0.938
p < 0.001
r = 0.918
p < 0.001
r = 0.871
p < 0.001
r = 0.811
p = 0.001
c
24-plex – 200-plex NULISAseq correlation
EGF
BDNF
IL17A
CCL13
IL10
IL4
IL5
IL16
TNFSF12
IL17C
TSLP
IFNA1; IFNA13
CCL20
FGF19
CXCL10
LIF
CXCL8
IFNL1
CCL22
IL6
IL13
IL20
CD200R1
CCL23
24−plex
200−plex
r = 0.997
p < 0.001
r = 0.996
p < 0.001
r = 0.995
p < 0.001
r = 0.995
p < 0.001
r = 0.993
p < 0.001
r = 0.992
p < 0.001
r = 0.992
p < 0.001
r = 0.988
p < 0.001
r = 0.988
p < 0.001
r = 0.985
p < 0.001
r = 0.983
p < 0.001
r = 0.983
p < 0.001
r = 0.981
p < 0.001
r = 0.98
p < 0.001
r = 0.979
p < 0.001
r = 0.977
p < 0.001
r = 0.976
p < 0.001
r = 0.975
p < 0.001
r = 0.961
p < 0.001
r = 0.958
p < 0.001
r = 0.953
p < 0.001
r = 0.943
p < 0.001
r = 0.938
p < 0.001
r = 0.918
p < 0.001

Figure 3

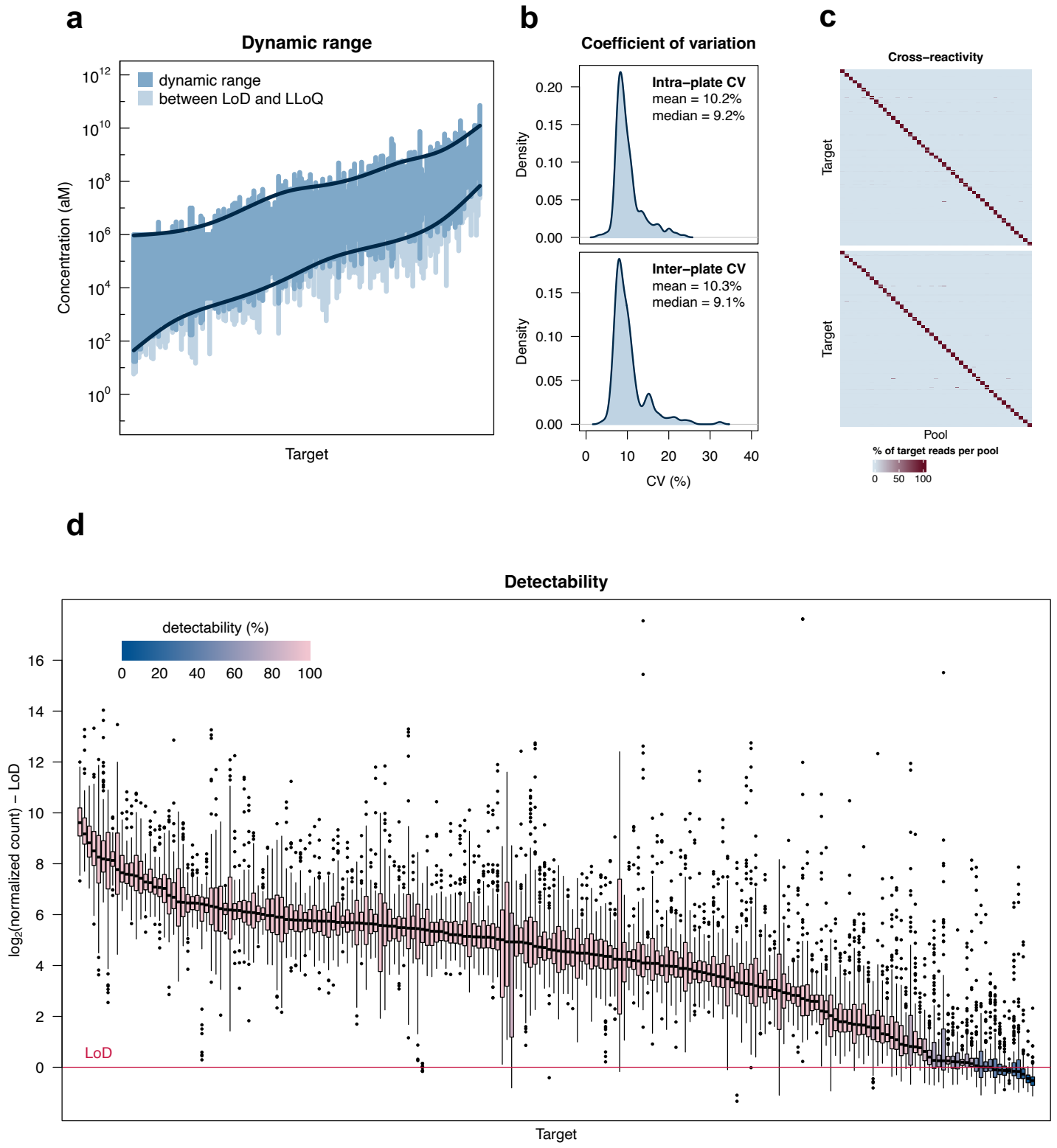
a
Dynamic range
dynamic range
between LoD and LLoQ
Concentration (aM)
Target
b
Coefficient of variation
Intra−plate CV
mean = 10.2%
median = 9.2%
Inter−plate CV
mean = 10.3%
median = 9.1%
Density
CV (%)
c
Cross−reactivity
Target
Pool
% of target reads per pool
d
Detectability
detectability (%)
log2(normalized count) − LoD
LoD
Target

Figure 4

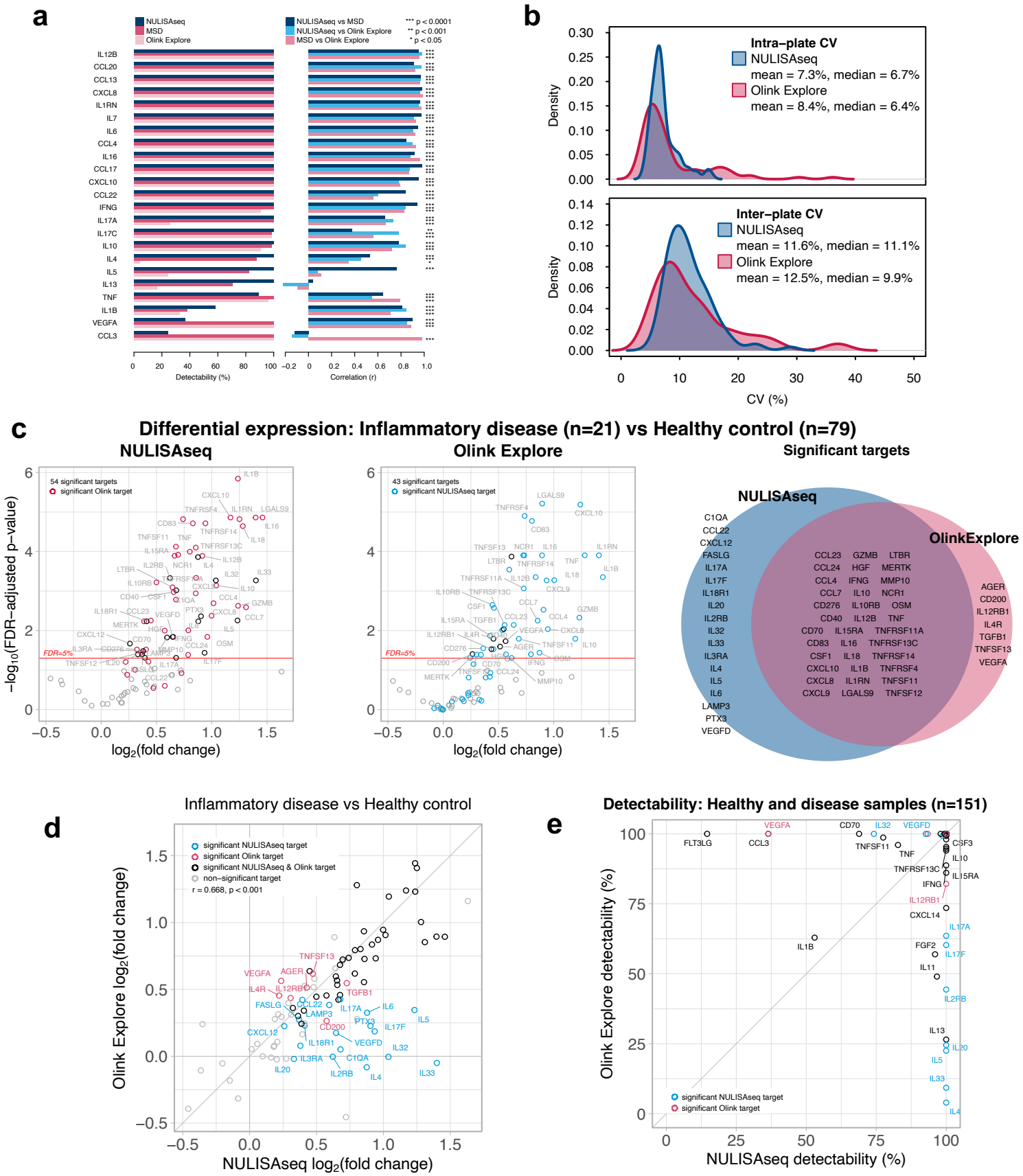
a
NULISAseq
MSD
Olink Explore
NULISAseq vs MSD
NULISAseq vs Olink Explore
MSD vs Olink Explore
*** p < 0.0001
** p < 0.001
* p < 0.05
Detectability (%)
Correlation (r)
b
Intra−plate CV
NULISAseq
mean = 7.3%, median = 6.7%
Olink Explore
mean = 8.4%, median = 6.4%
Inter−plate CV
NULISAseq
mean = 11.6%, median = 11.1%
Olink Explore
mean = 12.5%, median = 9.9%
Density
CV (%)
c
Differential expression: Inflammatory disease (n=21) vs Healthy control (n=79)
NULISAseq
54 significant targets
significant Olink target
FDR=5%
−log10(FDR−adjusted p−value)
log2(fold change)
Olink Explore
43 significant targets
significant NULISAseq target
Significant targets
NULISAseq
OlinkExplore
C1QA
CCL22
CXCL12
FASLG
IL17A
IL17F
IL18R1
IL20
IL2RB
IL32
IL33
IL3RA
IL4
IL5
IL6
LAMP3
PTX3
VEGFD
CCL23 GZMB LTBR
CCL24 HGF MERTK
CCL4 IFNG MMP10
CCL7 IL10 NCR1
CD276 IL10RB OSM
CD40 IL12B TNF
CD70 IL15RA TNFRSF11A
CD83 IL16 TNFRSF13C
CSF1 IL18 TNFRSF14
CXCL10 IL1B TNFRSF4
CXCL8 IL1RN TNFSF11
CXCL9 LGALS9 TNFSF12
AGER
CD200
IL12RB1
IL4R
TGFB1
TNFSF13
VEGFA
d
Inflammatory disease vs Healthy control
significant NULISAseq target
significant Olink target
significant NULISAseq & Olink target
non−significant target
r = 0.668, p < 0.001
Olink Explore log2(fold change)
NULISAseq log2(fold change)
e
Detectability: Healthy and disease samples (n=151)
significant NULISAseq target
significant Olink target
Olink Explore detectability (%)
NULISAseq detectability (%)

Figure 5

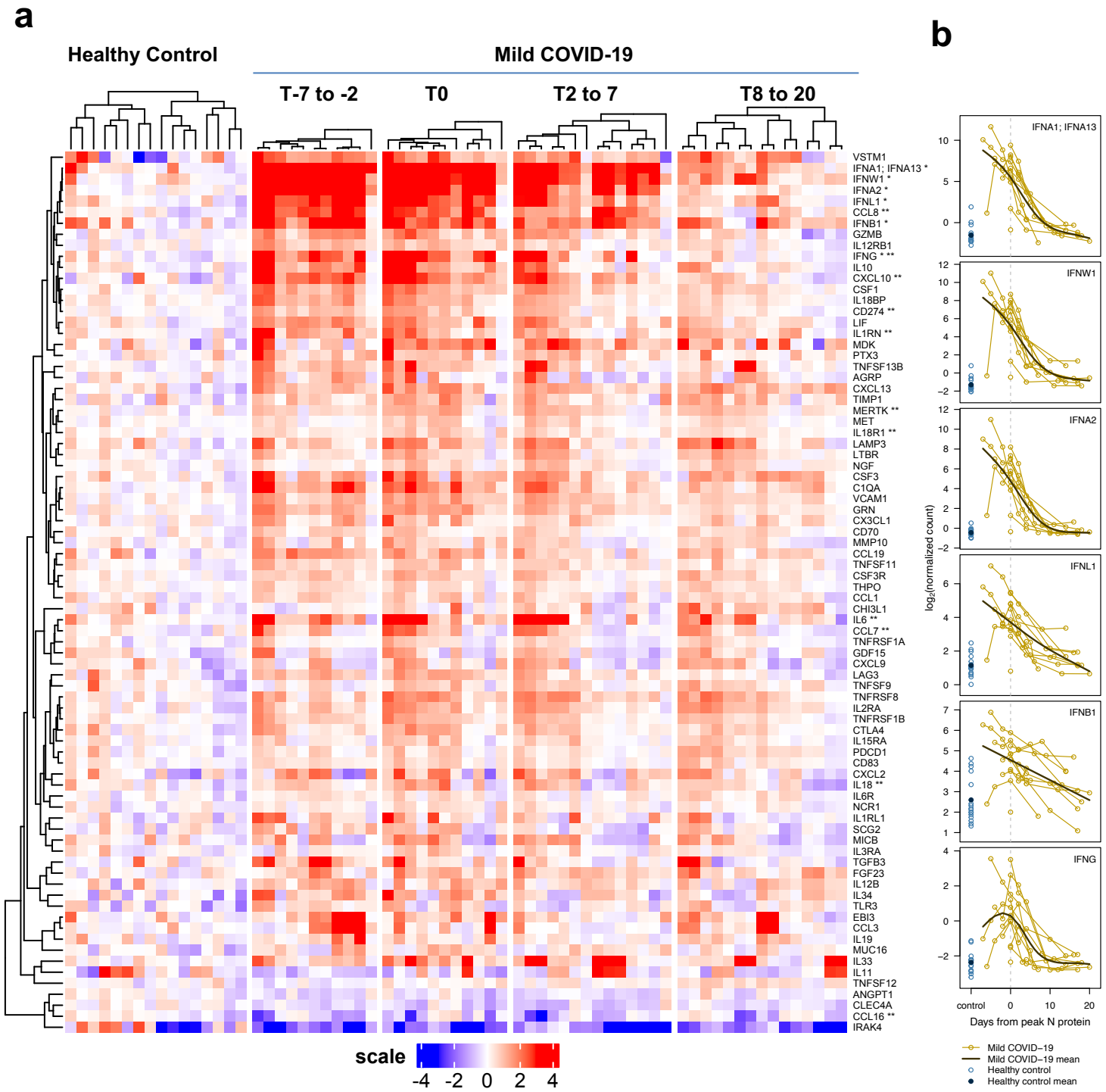
a
Healthy Control
Mild COVID-19
T-7 to -2
T0
T2 to 7
T8 to 20
VSTM1
IFNA1; IFNA13 *
IFNW1 *
IFNA2 *
IFNL1 *
CCL8 **
IFNB1 *
GZMB
IL12RB1
IFNG * **
IL10
CXCL10 **
CSF1
IL18BP
CD274 **
LIF
IL1RN **
MDK
PTX3
TNFSF13B
AGRP
CXCL13
TIMP1
MERTK **
MET
IL18R1 **
LAMP3
LTBR
NGF
CSF3
C1QA
VCAM1
GRN
CX3CL1
CD70
MMP10
CCL19
TNFSF11
CSF3R
THPO
CCL1
CHI3L1
IL6 **
CCL7 **
TNFRSF1A
GDF15
CXCL9
LAG3
TNFSF9
TNFRSF8
IL2RA
TNFRSF1B
CTLA4
IL15RA
PDCD1
CD83
CXCL2
IL18 **
IL6R
NCR1
IL1RL1
SCG2
MICB
IL3RA
TGFB3
FGF23
IL12B
IL34
TLR3
EBI3
CCL3
IL19
MUC16
IL33
IL11
TNFSF12
ANGPT1
CLEC4A
CCL16 **
IRAK4
scale
-4 -2 0 2 4
b
IFNA1; IFNA13
IFNW1
IFNA2
IFNL1
IFNB1
IFNG
log2(normalized count)
control
0
10
20
Days from peak N protein
Mild COVID−19
Mild COVID−19 mean
Healthy control
Healthy control mean

List of Supplementary Materials

Supplementary Tables

Table S1. List of 3 additional antigen pools for evaluating cross reactivity to homologous proteins not in the NULISAseq 200plex Inflammation Panel

CEACAM5 50% homology pool	**IFNA1 50% homology pool**	**70% homology pool**
CEACAM3	IFNA8	LGALS9B
CEACAM6	IFNA10	CCL3L1
CEACAM8	IFNA21	CCL4L1
CEACAM1	IFNA5	HPCAL4
CEACAM7	IFNA14	IFNA5
PSG9	IFNA17	CXCL6
PSG11	IFNA7	FTMT
PSG2	IFNA6	WNT7B
	IFNA4	IFNL3
	IFNA16	CD200R1L
		CEACAM1

Table S2. Sample sets and disease group categories used in NULISAseq verification studies

Disease type	Primary diagnosis	Sample Set 1 n=74	Sample Set 2 n=77
Healthy (n=79)		39	40
Total disease (n=72)		35	37
Cancer (n=32)	Bladder cancer (n=2)	1	1
	Breast cancer (n=2)	2	0
	Cervical cancer (n=1)	0	1
	Colorectal cancer (n=1)	1	0
	Gastric cancer (n=1)	0	1
	Head & neck cancer (n=5)	3	2
	Leukemia (n=3)	2	1
	Lung cancer (n=5)	2	3
	Lymphoma (n=6)	3	3
	Melanoma (n=1)	0	1
	Myeloma (n=3)	1	2
	Pancreatic cancer (n=2)	2	0
Inflammatory disease (n=21)	Rheumatoid arthritis (n=5)	2	3
	Sjögren's Syndrome (n=5)	3	2

	Systemic lupus erythematosus (n=5)	3	2
	Ulcerative colitis (n=6)	4	2
Kidney disease (n=4)	Chronic kidney disease (n=4)	2	2
Metabolic disease (n=9)	Type I diabetes (n=7)	3	4
	Type II diabetes (n=2)	1	1
Neurological disease (n=6)	Alzheimer's disease (n=1)	0	1
	Parkinson's disease (n=5)	3	2

Table S3. Sample characteristics for the comparison of NULISAseq with other immunoassays

	Healthy controls (n=79)	Patients with disease (n=72)
Age in years (mean (sd)) *	46.7 (10.3)	64.0 (14.1)
Female (n (%))	34 (43.0%)	42 (58.3%)
Disease group (n (%))		
Cancer		32 (44.4%)
Inflammatory disease		21 (29.2%)
Kidney disease		4 (5.6%)
Metabolic disease		9 (12.5%)
Neurological disease		6 (8.3%)

* Age information was missing for one healthy male participant; this was imputed using the mean age for healthy males. Age information was missing for one male patient with a cancer diagnosis; this was imputed using the mean age of male patients with cancer.

Table S4. Detectability of 92 shared targets of the NULISAseq 200-plex and Olink Explore 384 Inflammation panels in 79 samples from healthy controls and 72 samples from patients with different diseases

.

Panel	All samples (n=151)	Healthy controls (n=79)	Patients with disease (n=72)
	n (%) detectable* targets		
NULISAseq	89 (96.7%)	89 (96.7%)	89 (96.7%)
Olink Explore	85 (92.4%)	86 (95.3%)	85 (92.4%)
	detectability (%): mean (sd)/median [min, max]		
NULISAseq	95.9 (14.3)/100.0 [14.6, 100.0]	95.4 (15.8)/100.0 [3.8, 100.0]	96.4 (12.7)/100.0 [26.4, 100.0]
Olink Explore	91.6 (21.3)/100.0 [4.0, 100.0]	91.1 (22.0)/100.0 [1.3, 100.0]	92.2 (20.7)/100.0 [6.9, 100.0]

* A detectable target was defined as one for which the values were above the limit of detection for >50% of samples. The detectability was calculated as the percentage of samples in which the target signal was above the LOD.

Table S5. Sample characteristics for the characterization of the host response to SARS-CoV-2 infection with NULISAseq

	Healthy controls (n=16)	Patients with mild COVID-19 (n=11)
Age in years (mean (sd))	57.3 (13.6)	51.4 (20.6)
Female (n (%))	7 (43.8%)	8 (72.7%)
		Number of observations for each time period
t_{-1} (2-7 days before t_0*)		11
t_0		11
t_1 (2-7 days after t_0)		14
t_2 (8-20 days after t_0)		15

*t_0 was the time point at which the SARS-CoV-2 Nucleocapsid (N)protein level was maximum.

Supplementary Figures

Fig. S1. Specificity of the NULISA assay for human EGFR in the presence of mouse Egfr. **a**, Limit of detection for human EGFR measured in the presence of 0, 1, 10, and 100 pM mouse Egfr. **b**, NULISA signal of 10 pM human EGFR, 10 pM mouse Egfr, and the blank control.

Fig. S2a. Sensitivity, sample detection and accuracy of the NULISA NfL assay and correlation with Quanterix SIMOA results. **a**, Representative standard curve of the NULISA NfL assay. **b**, NfL detection in plasma, serum, cerebrospinal fluid (CSF) samples from healthy donors and Alzheimer's (AD) and Parkinson's (PD) patients. The red line indicates the functional LOD. The functional LoD was the LoD after accounting for sample dilution. **c**, Correlation between NULISA and SIMOA NfL assay results with different antibody pairs. **Table**, NULISA NfL percent recovery for various assay parameters (spike recovery, dilutional linearity, and parallelism).

Fig. S2b. Sensitivity, spike recovery, linearity and parallelism of the NULISA IL1B assay. **a**, Representative standard curve of the NULISA IL1B assay. **b**, IL1B detection in plasma (n=13) and serum (n=14) samples from healthy donors. The red line indicates the functional LOD. **Table**, NULISA IL1B percent recovery (mean and range) for various assay parameters (spike recovery, dilutional linearity, and parallelism).

Fig. S2c. Sensitivity, spike recovery, linearity and parallelism of the NULISA IL6 assay. **a**, Representative standard curve of the NULISA IL6 assay. **b**, IL6 detection in plasma samples from healthy donors. The red line indicates the functional LOD. **Table**. NULISA IL6 assay percent recovery (mean and range) for various assay parameters (spike recovery, dilutional linearity, and parallelism).

Fig. S3. Signal tuning for multiplex NULISAseq assay. Standard curves of the IL4 assay were generated using different hot:cold antibody ratios. The total concentrations of both capture (aC) and detection (aD) antibodies after mixing were maintained the same for all conditions. The percentages of hot-capture and detection antibodies used to generate each curve are indicated. Six levels of protein calibrators were used to assess the signal reduction in each condition when cold antibody was added.

Fig. S4. Detectability of 92 common targets shared between the NULISAseq 200-plex and the Olink Explore 384 Inflammation Panel. Detectability was calculated for each target as the percentage of samples with results above the LOD using 79 samples from healthy controls (left) or 72 samples from patients with different diseases (right).

Fig. S5. Differential expression analysis comparing n=32 patients with cancer and n=79 healthy controls using 92 shared targets between the NULISAseq 200-plex Inflammation Panel and the Olink Explore 384 Inflammation Panel. **a,** Volcano plots of the estimated log2-fold changes vs. the FDR-adjusted p value from the linear model, adjusted for age, sex, and plate. Left, NULISAseq; middle, Olink; right, overlap of significant targets between NULISAseq and Olink Explore. **b,** Pearson correlation of the estimated log2-fold changes between NULISAseq and Olink Explore.

Fig. S6. Select low-abundance targets associated with autoimmune diseases detected by NULISAseq but not by Olink Explore. Boxplots show the distributions of residuals (after adjusting for age, sex, and plate) for healthy controls versus inflammatory disease subgroups. FDR-adjusted p values were obtained based on the disease status (inflammatory disease, n=21, versus healthy control, n=79) coefficient from linear models (adjusted for age, sex, and plate) used in the differential expression analysis of 92 shared NULISAseq and Olink targets. RA: rheumatoid arthritis (n=5), SjS: Sjögren's syndrome (n=5), SLE: systemic lupus erythematosus (n=5), UC: ulcerative colitis (n=6).

Supplementary Data Files

Supplementary Data A. NULISAseq 200-plex Inflammation Panel and performance summary (precision, LOD, dynamic range, detectability, and specificity). The column "Hot/cold signal tuning" indicates whether the assay sensitivity for the target was tuned down with hot/cold antibody mixing, which would result in higher LODs but shoud maintain sample detectability.

Supplementary Data B. Detailed results obtained by comparing NULISAseq and Olink Explore. Columns with names ending with "_coef", "_pval" and "_FDR" list the regression coefficients (log2-fold change), unadjusted p values and FDR-adjusted p values, respectively, from linear models assessing differential expression between 79 samples from healthy controls and 21 samples from patients with inflammatory disease or 32 samples from patients with cancer, adjusted for age, sex, and plate. Columns with names containing "detect" list target detectability, based on the same samples from 79 healthy controls and an expanded set of 72 samples from patients with various diseases, and those with names containing "CV" list intra- and interplate CV%.

Supplementary Data C. Detailed differential expression analysis results for the comparison of samples from patients with mild COVID-19 and healthy donors. Sheet 1 (limma_analysis) lists the full results with the log2(fold change) and FDR-adjusted p values; sheet 2 (limma_results_top20)

lists the top 20 significantly different targets ranked by maximum fold change; and sheet 3 (Enrichment) lists the pathway analysis results based on all significantly different targets.

S1. EGFR assay specificity

a

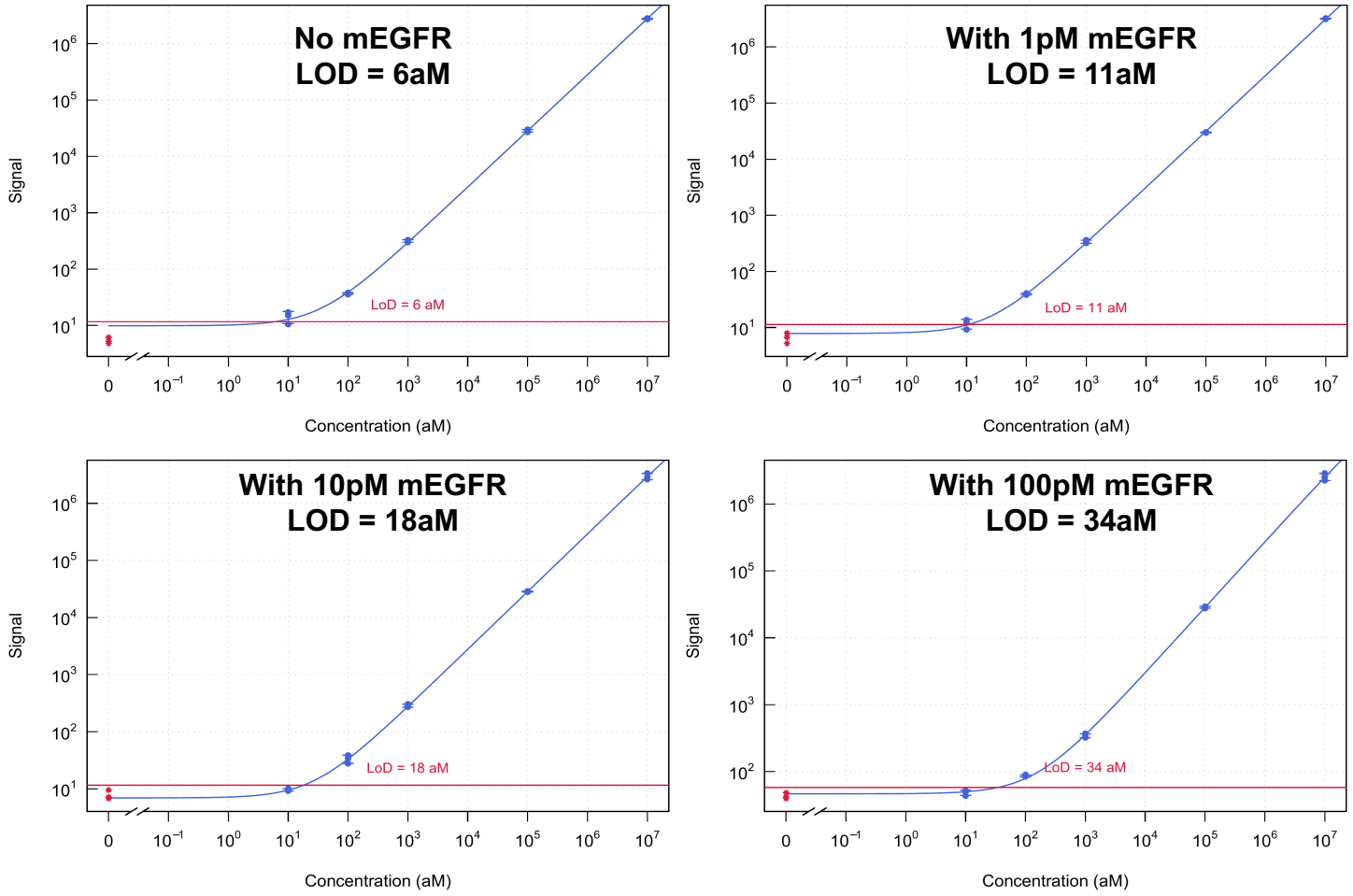

b

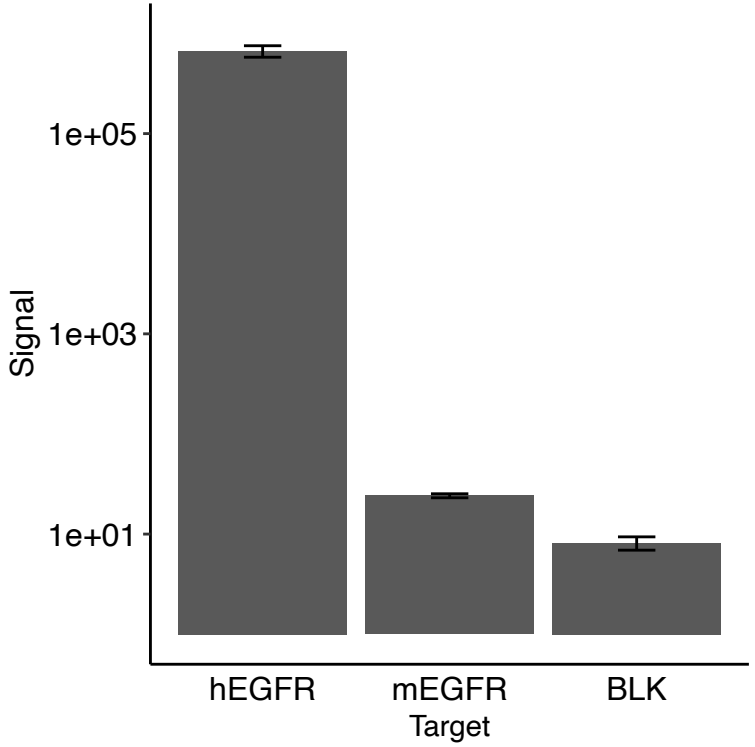

S2a. Sensitivity, spike-recovery, linearity and parallelism of NULISA NfL assay and correlation with SIMOA assay

a) Representative NfL NULISA standard curve

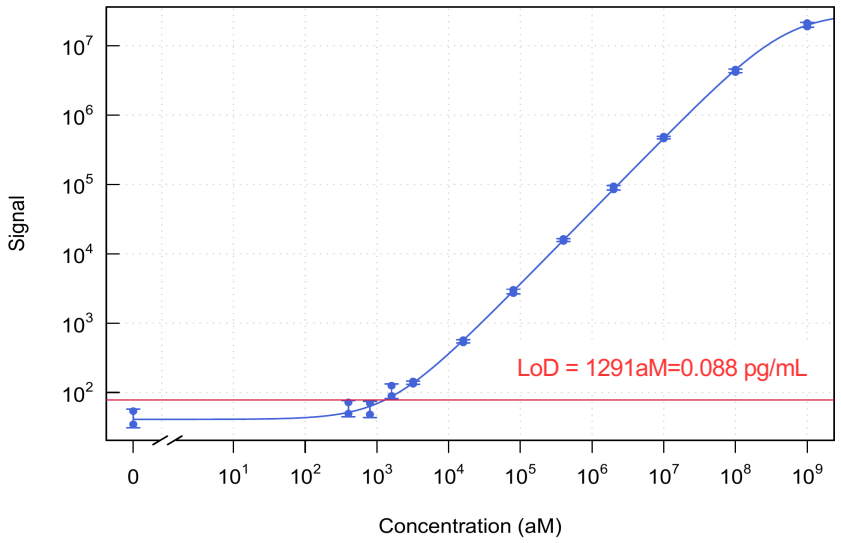

b) NfL sample detection

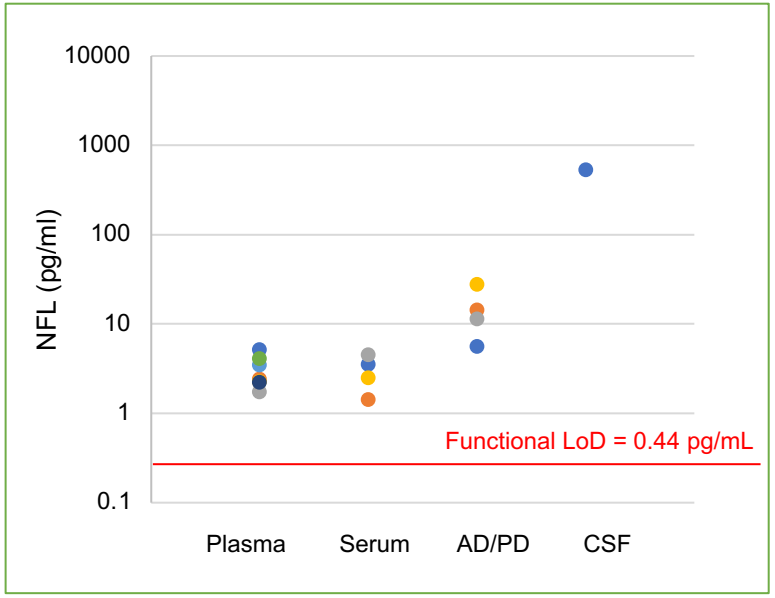

c) NULISA and SIMOA correlation

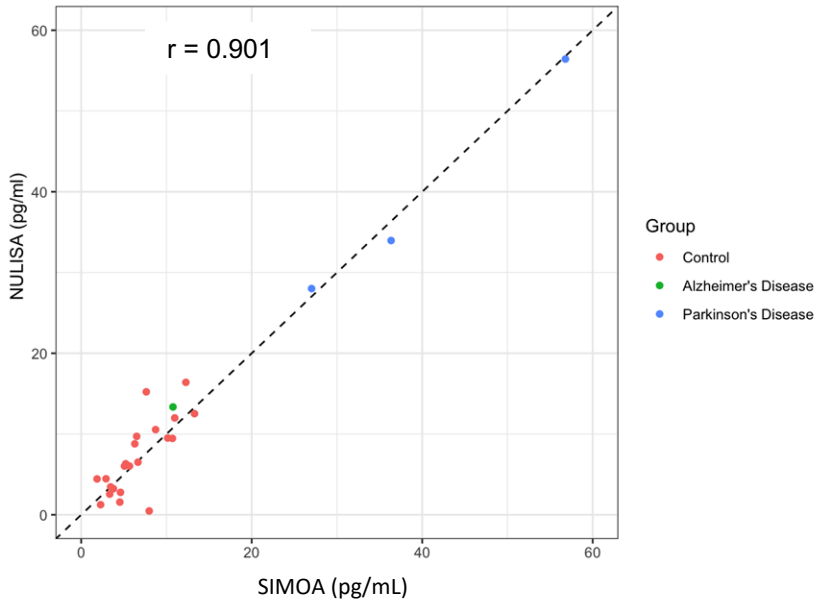

Spike and Recovery	Mean = 88%	Range = 67-103%
Dilution Linearity	Mean = 97%	Range = 68-113%
Parallelism	Mean = 110%	Range = 105-117%

S2b. Sensitivity, spike-recovery, linearity and parallelism of NULISA IL1B assay

a) Representative IL1B Standard Curve

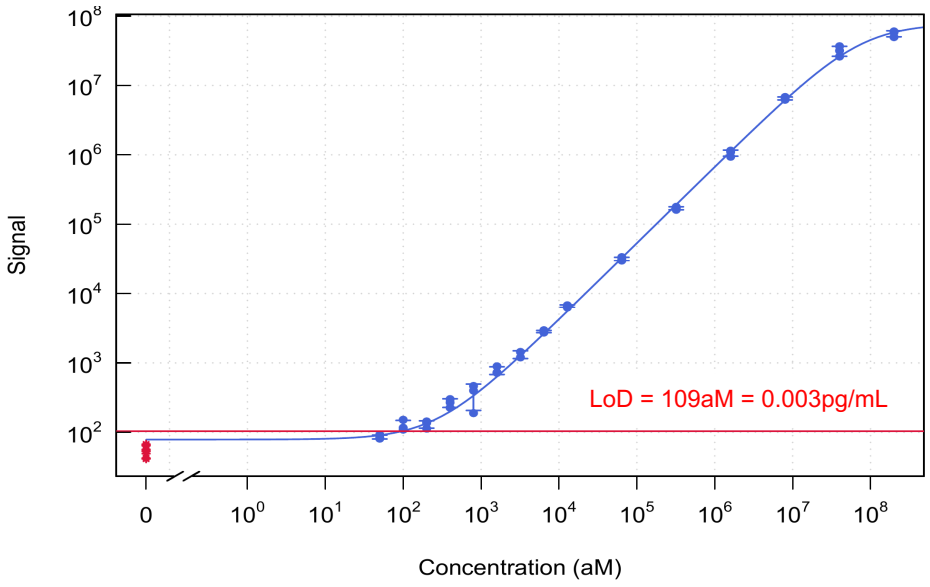

b) IL1B sample detection

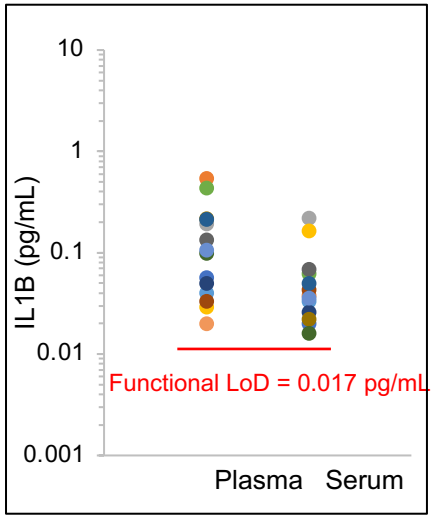

Spike Recovery	Mean = 98.6%	Range = 93 -109%
Dilutional Linearity	Mean = 96%	Range = 86 -101%
Parallelism	Mean = 98 %	Range = 77-123%

S2c: Sensitivity, spike-recovery, linearity and parallelism of NULISA IL6 assay

a) Representative IL6 Standard Curve

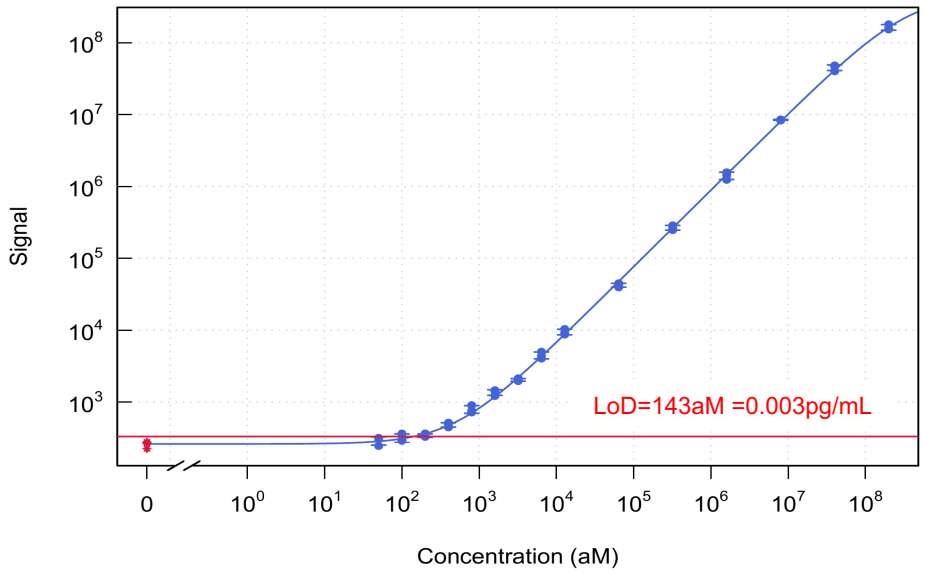

b) IL6 sample detection

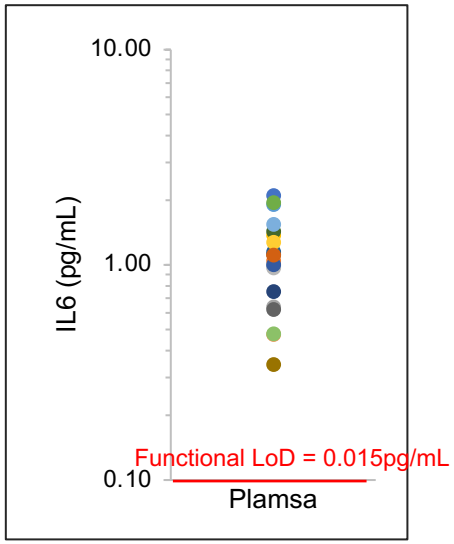

Spike Recovery	Mean = 92%	Range =81-105 %
Dilutional Linearity	Mean = 117%	Range = 102 -138%
Parallelism	Mean = 115 %	Range = 88-135%

S3. Hot / cold antibody tuning

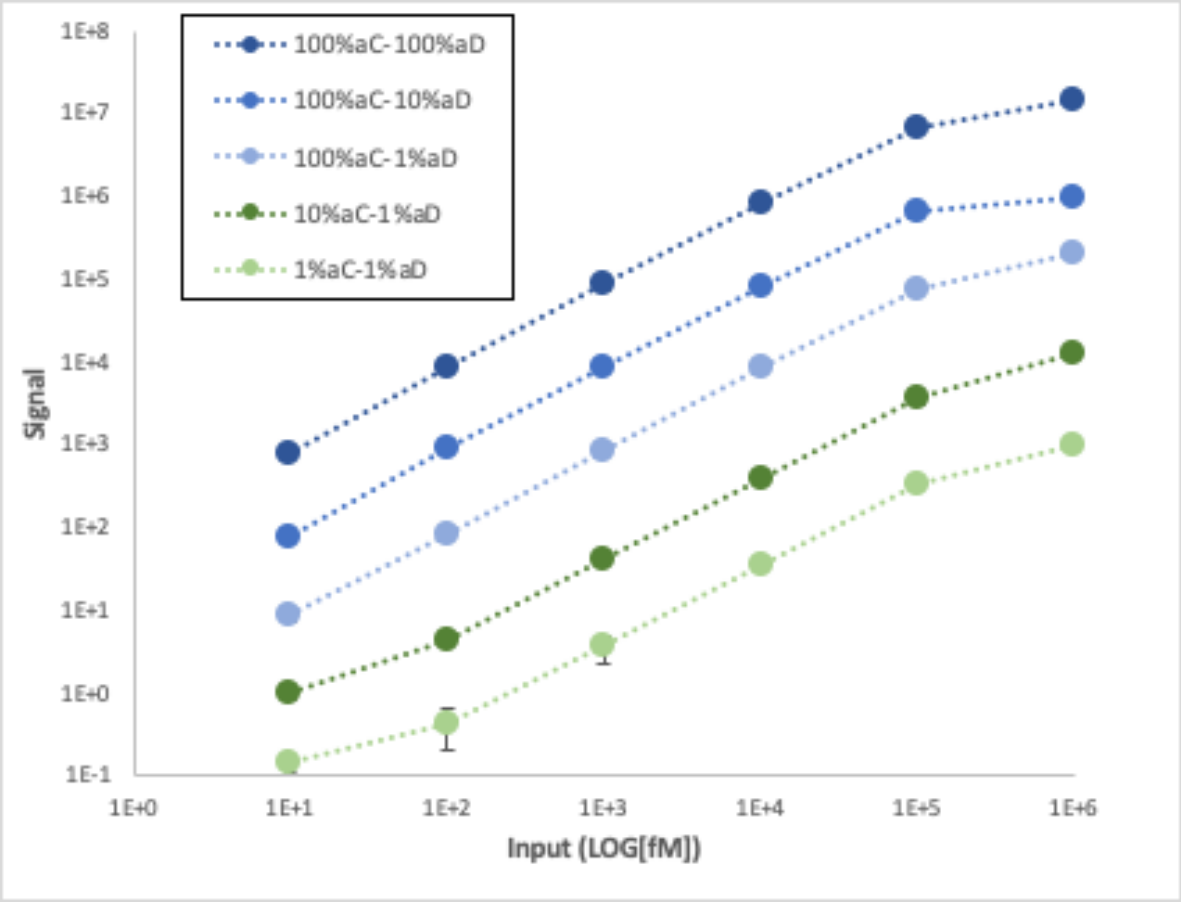

S4. NULISAseq showed better detectability for more of the 92 shared targets as compared with Olink Explore

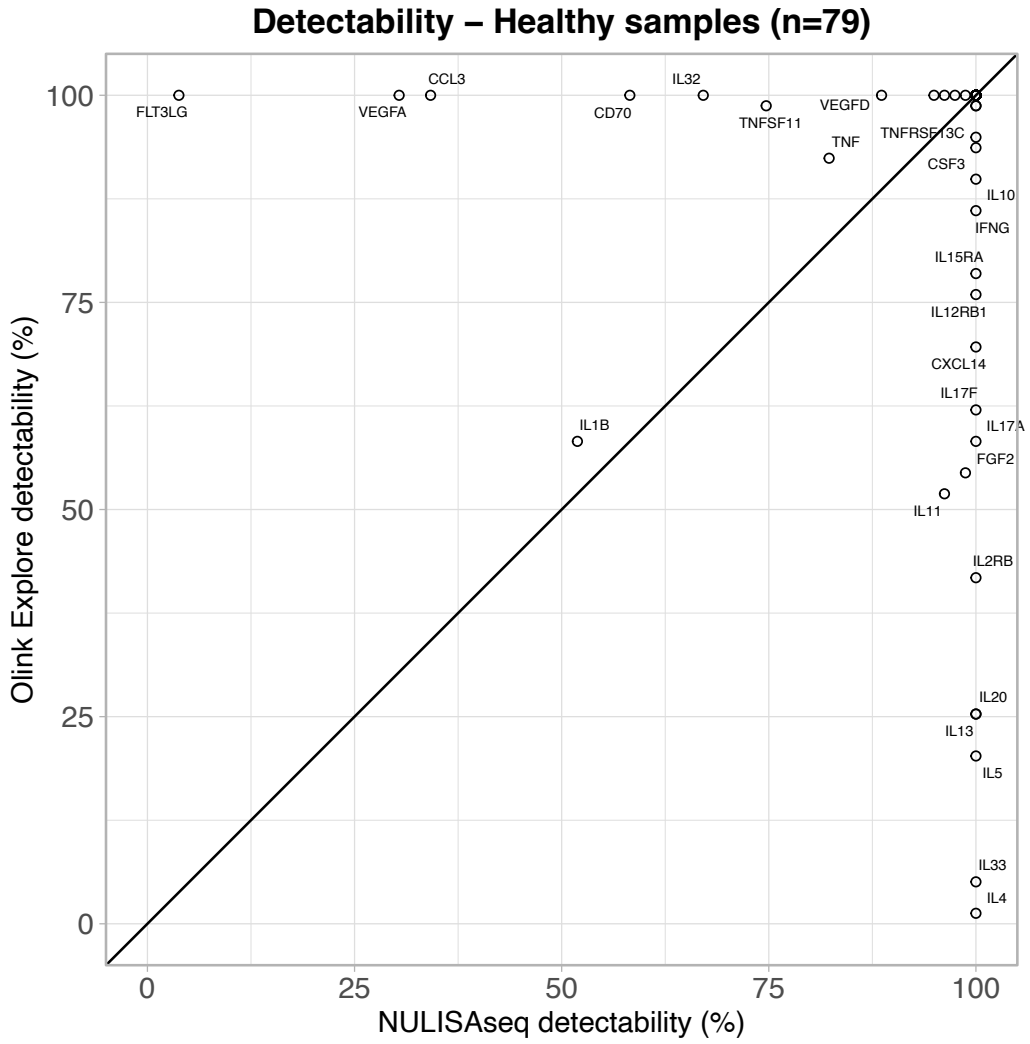

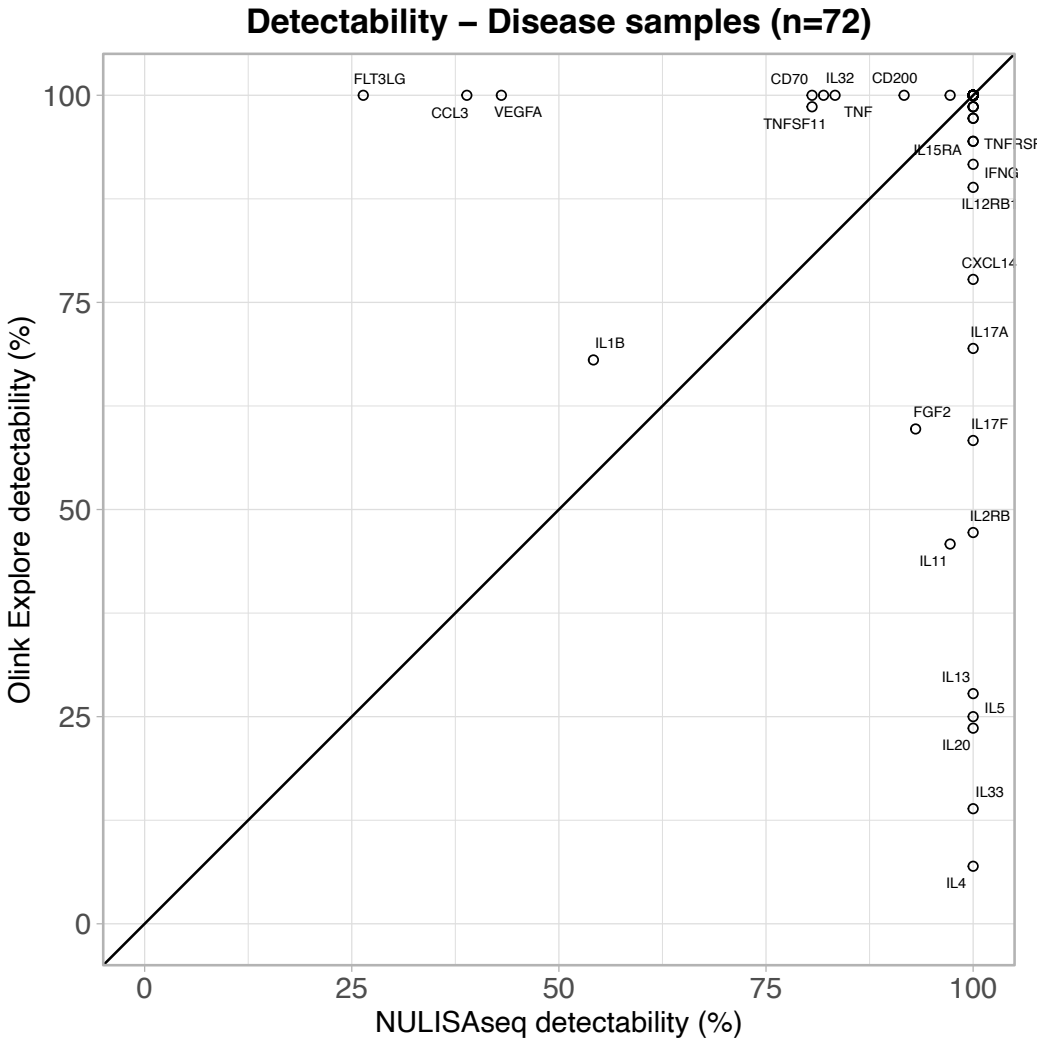

S5. Cancer differential expression, NULISAseq versus Olink, 92 shared targets

a

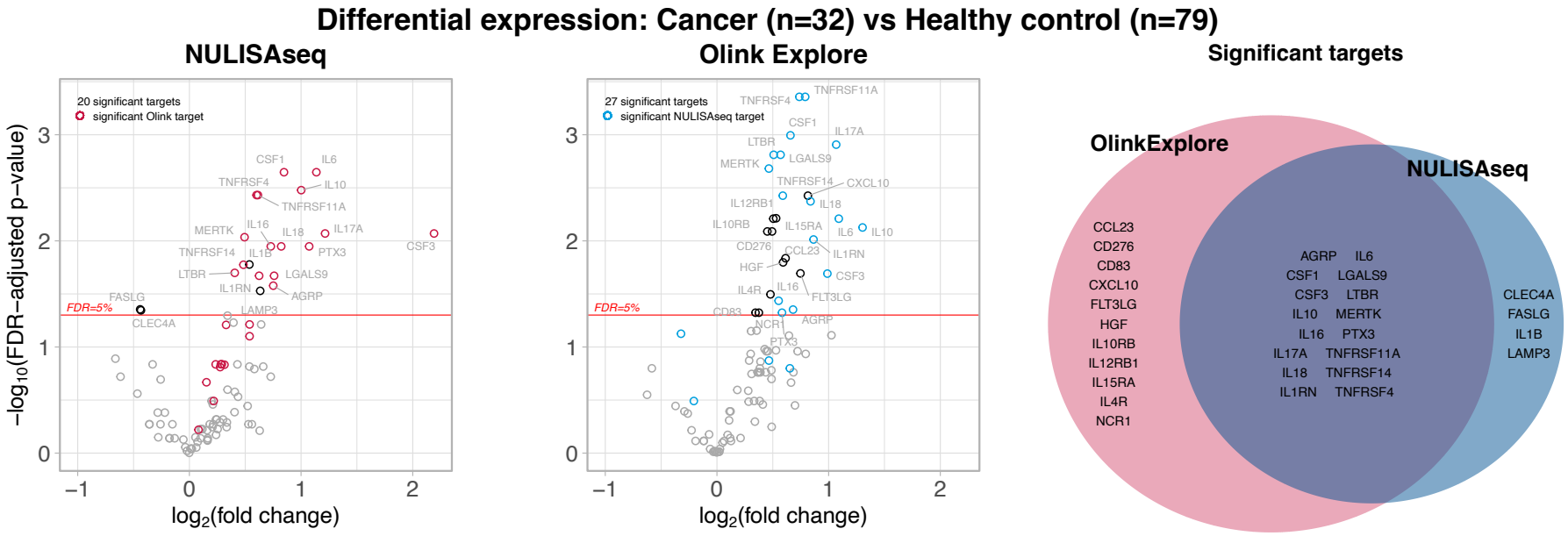

b

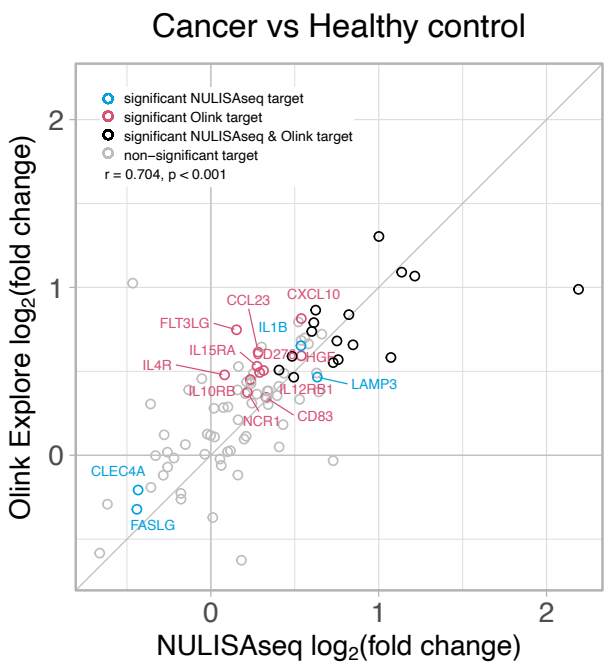
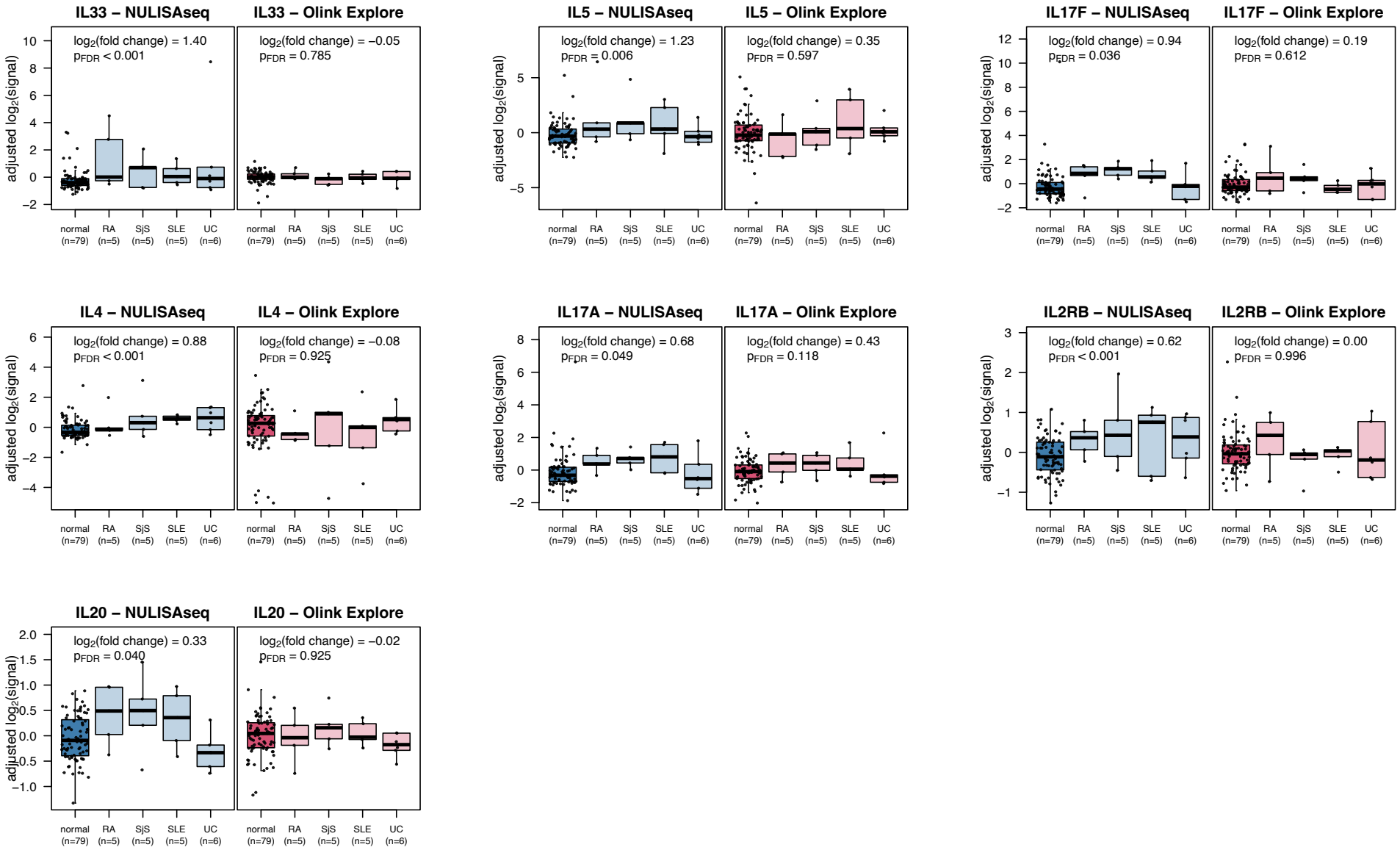
S6. Targets associated with autoimmune diseases detected by NULISAseq but not by Olink Explore